chromosome 3 clone RP11-61K12 (AC011199). We synthesized gene-specific primers and genotyped each individuals by PCR-SSCP analysis. The genotype frequency of the 82133G>A polymorphism of human chromosome 3 clone RP11-61K12 (AC011199) differed significantly (P= 0.0189, Fisher's exact test) between older subjects (>90 years) and younger subjects (<70 years) (Table 2). Differences in allele and genotype frequencies between the four age categories were not statistically significant.

The SNP was located in a mammalian-wide interspersed repeat (MIR) on chromosome 3 and was described in GeneBank. MIRs are one of the most common interspersed repeats in primates, with an estimated 300,000 copies per genome that account for 1–2% of the total DNA [6]. It is not clear whether this SNP is associated with longevity; however, it is noteworthy that the strategy we describe herein was useful for identifying an SNP that showed statistically significant differences in its distribution across the subject groups.

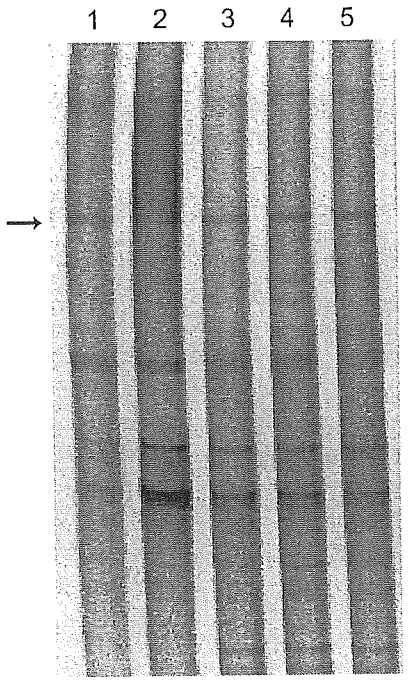

Fig. 1. Electropherogram of AP-PCR-SSCP. The AP-PCR product amplified by using Ae6R primer was separated by SSCP analysis (6% polyacrylamide gel electrophoresis at 15 °C for 5 h). A stained band with different mobility and density (shown as arrow; observed as slightly broad band in lane 1) was excised from the gel, cloned, and sequenced. As a result of sequential examinations, an SNP of the human chromosome 3 clone was found. Lane 1, individuals aged more than 100 years (n=9); lanes 2–4, individuals aged 90–99 years (3 sub-groups, n=8 each group); lane 5, individuals aged 60–69 years (n=9).

Table 2
Genotype and allele frequencies of the 82133G>A polymorphism on human chromosome 3 clone RP11-61K12 (AC011199) in subjects classified by age

Age	Genotype			G allele		A allele	
	G/G	G/A	A/A	No.	%	No.	%
≥100 years	4	5	0	13	72	5	28
90–99 years	10	11	0	31	74	11	26
60–69 years	1	6	2	8	44	10	56
<30 years	9	13	5	31	57	23	43
>90 years	13*	16*	0*	44	73	16	27
<70 years	10*	19*	7*	39	54	33	46

* The genotype frequency differed significantly (P=0.0189, Fisher's exact test) between older subjects (>90 years) and younger subjects (<70 years).

In the present pilot study, we used mini-gel, for SSCP. If large gels with long separations or 2-dimensional separation with detection by fluorescence dyes are used, better resolution could be obtained. Both the phenotype-to-genotype screening strategy and semi-quantitative distribution measurement using pooled DNA may be useful in screening for important genetic variations associated with a variety of human diseases and phenotypes. The advanced improvement of precise techniques is clearly necessary, however, the pooled DNA strategy and quantitative genotype discrimination can also indicate the relative proportion of different genotypes, haplotypes or allelotypes at glance and be applied to screening for the relationship between phenotype and genotype more effectively.

Acknowledgements

This research was supported in part by Health and Labor Sciences Research Grants for Third Term Comprehensive Control Research for Cancer (H15-9 and H16-018), by Grants-in-Aid for Exploratory Research (15659133) from the Japan Society for the Promotion of Science, and by the Nakatani Electronic Measuring Technology Association of Japan.

References

[1] Um J-Y, Lee K-M, Kim H-M. Polymorphism of interleukin-1 receptor antagonist gene and obesity. Clin Chim Acta 2004; 340:173–7.
[2] Welsh J, McClelland M. Fingerprinting genomes using PCR with arbitrary primers. Nucleic Acids Res 1990;18:7213–8.
[3] Peinado MA, Malkhosyan S, Velazquez A, Perucho M. Isolation and characterization of allelic losses and gains in colorectal tumors by arbitrarily primed polymerase chain reaction. Proc Natl Acad Sci U S A 1992;89:10065–9.
[4] Maekawa M, Sugano K, Ushiama M, Masuda T, Ohkura H, Kakizoe T, et al. Relative ratios of mRNA molecules encoded by genes with homologous sequences using fluorescence-based single-strand conformation polymorphism analysis. Biochem Biophys Res Commun 1996;223:520–5.
[5] National Center for Biotechnology Information. BLAST. http://www.ncbi.nlm.nih.gov/BLAST/.
[6] Smit AF, Riggs AD. MIRs are classic, tRNA-derived SINEs that amplified before the mammalian radiation. Nucleic Acids Res 1995;23:98–102.

We thank Herman ten Brink and Rob Ofman for helpful technical suggestions and discussion. This work was supported by grants from the Netherlands Organization for Scientific Research (NWO-MW: No. 903-42-077), the European Leukodystrophy Association, and European Union Project LSHM-CT-2004-502987.

References

1. Singh I, Moser AE, Goldfischer S, Moser HW. Lignoceric acid is oxidized in the peroxisome: implications for the Zellweger cerebro-hepato-renal syndrome and adrenoleukodystrophy. Proc Natl Acad Sci U S A 1984;81:4203–7.
2. Singh I, Moser AE, Moser HW, Kishimoto Y. Adrenoleukodystrophy: impaired oxidation of very long chain fatty acids in white blood cells, cultured skin fibroblasts, and amniocytes. Pediatr Res 1984;18:286–90.
3. Lazo O, Contreras M, Hashmi M, Stanley W, Irazu C, Singh I. Peroxisomal lignoceroyl-CoA ligase deficiency in childhood adrenoleukodystrophy and adrenomyeloneuropathy. Proc Natl Acad Sci U S A 1988;85:7647–51.
4. Wanders RJ, van Roermund CW, van Wijland MJ, Schutgens RB, van den BH, Schram AW, et al. Direct demonstration that the deficient oxidation of very long chain fatty acids in X-linked adrenoleukodystrophy is due to an impaired ability of peroxisomes to activate very long chain fatty acids. Biochem Biophys Res Commun 1988;153:618–24.
5. Wanders RJ, Denis S, Ruiter JP, Schutgens RB, van Roermund CW, Jacobs BS. Measurement of peroxisomal fatty acid β-oxidation in cultured human skin fibroblasts. J Inherit Metab Dis 1995;18 Suppl 1:113–24.
6. Watkins PA, Ferrell EV Jr, Pedersen JI, Hoefler G. Peroxisomal fatty acid β-oxidation in HepG2 cells. Arch Biochem Biophys 1991;289:329–36.
7. Valianpour F, Selhorst JJ, van Lint LE, van Gennip AH, Wanders RJ, Kemp S. Analysis of very long-chain fatty acids using electrospray ionization mass spectrometry. Mol Genet Metab 2003;79:189–96.
8. Gootjes J, Mooijer PA, Dekker C, Barth PG, Poll-The BT, Waterham HR, et al. Biochemical markers predicting survival in peroxisome biogenesis disorders. Adv Exp Med Biol 2003;544:67–8.

DOI: 10.1373/clinchem.2004.038539

High Lactate Dehydrogenase Isoenzyme 1 in a Patient with Malignant Germ Cell Tumor Is Attributable to Aberrant Methylation of the *LDHA* Gene

Jinko Ishikawa,[1] *Terumi Taniguchi,*[1] *Hitomi Higashi,*[1] *Katsutoshi Miura,*[2] *Kazuya Suzuki,*[3] *Akihiro Takeshita,*[1] *and Masato Maekawa*[1]* ([1] Department of Laboratory Medicine, [2] Department of Pathology, and [3] First Department of Surgery, Hamamatsu University School of Medicine, Hamamatsu 431-3192, Japan; * author for correspondence: fax 81-53-435-2794, e-mail mmaekawa@hama-med.ac.jp)

Lactate dehydrogenase (LD; EC 1.1.1.27) isoenzymes are formed by random combinations of two different subunits encoded by structurally distinct genes, *LDHA* and *LDHB (1)*. Expression of mammalian *LDHA* and *LDHB* is regulated during development and is tissue specific; therefore, alterations in the serum LD isoenzyme pattern serve as indicators of pathologic conditions and cancer development (*2*). Different phenotypes of LD isoenzyme patterns in cancer patients may originate from changes in expression of *LDHA* or *LDHB* caused by other regulatory genes or promoter methylation or from mutations involving deletions, duplications, or increased copy numbers. We previously observed in a retinoblastoma cell line a high proportion of LD1 with an extra band that migrated between LD2 and LD3. The unique LD isoenzyme pattern was attributable in part to transcriptional silencing by hypermethylation of the *LDHA* promoter (*3*). We also found that the increased concentrations of electrophoretically slow-moving LD isoenzymes in many gastric cancer cell lines are attributable to transcriptional silencing of *LDHB* expression by aberrant promoter methylation (*4*).

We recently encountered a male patient with mediastinal germ cell tumor who showed high serum LD activity and high LD1 isoenzyme activity. In germ cell tumors, increased LD1 concentrations often correlate with total copy number for the short arm of chromosome 12, which is where *LDHB* is located (*5*), but not all germ cell tumors show this increased copy number for chromosome 12. We therefore hypothesized that the high LD1 isoenzyme activity could be caused by aberrant methylation of the *LDHA* promoter.

The patient, a 21-year-old man, was admitted to our hospital because of fever and abnormal chest x-ray results. Laboratory tests revealed increased serum LD activity (299 U/L; reference interval, 101–193 U/L). Serum α-fetoprotein was increased to 2535 μg/L (reference interval <10 μg/L). The LD profiles included increased LD1 (49%) and a high LD1/LD2 ratio (2.2; Table 1). Chest x-ray examination revealed a mediastinal tumor. A pathology examination revealed that the tumor consisted of a combined malignant germ cell tumor (yolk sac tumor plus embryonal carcinoma plus dysgerminoma) with a focal rhabdomyosarcoma component arising from a mature cystic teratoma of the mediastinum (size, 8 × 8 × 4.8 cm). After surgical resection of the pulmonary metastasis, total LD activity decreased, but the LD isoenzyme pattern with high LD1 activity remained. After surgical resection of the primary tumor followed by high-dose chemotherapy, both the total LD activity and the LD isoenzyme pattern returned to normal (Table 1).

LD activity was measured by spectrophotometric assay on a Hitachi 7350 automated biochemistry analyzer (Hitachi High Technologies). Assay conditions were based on the method recommended by the Japanese Society of Clinical Chemistry (*6*). LD isoenzymes in serum were separated electrophoretically with Titan III support medium (Helena Laboratory).

Genomic DNA was extracted from the formalin-fixed, paraffin-embedded specimens of the surgically resected pulmonary metastasis and the primary mediastinal tumor with DNA isolation reagents (DNeasy Tissue Kit; Qiagen). For methylation analysis, we used methylation-specific PCR (MSP) (*7*). The sequences of primers specific for the methylated allele of *LDHA* were 5′-CGATTTCGGATTTTATTGTTACGC-3′ (forward) and 5′-CGCCCATCCCTCTACCCGTACG-3′ (reverse); those for the unmethylated allele were 5′-TATTTAAGTAGGGGTTGAAAGTTT-3′ (forward) and 5′-ACCTCAAATTTTACACCACCG-3′ (reverse; see Fig. 1 in the Data Supplement that accompanies the online version of this Technical Brief at http://www.clinchem.org/content/vol50/issue10/). The MSP-amplified products were confirmed by single-strand DNA conformation polymorphism (SSCP) analysis (*8*) and DNA sequencing analysis.

Table 1. Patient's lactate dehydrogenase profile and α-fetoprotein concentrations on various dates during 2003.

Test	Reference interval	Jan. 16	Feb. 11[a]	Feb. 27	March 18	June 12	Aug. 5[b]	Oct. 1[c]
LD, U/L	101–193	299	307	166	143	177	161	110
LD1, %	20.0–31.0	48.6		22.9		39.8		23.2
LD2, %	28.8–37.0	22.0		23.5		32.7		35.2
LD3, %	21.5–27.6	13.8		17.5		16.0		25.3
LD4, %	6.3–12.4	7.8		13.0		4.8		9.1
LD5, %	5.4–13.2	7.8		23.1		6.8		7.2
LD1/LD2	0.60–0.93	2.2		1.0		1.2		0.7
AFP,[d] μg/L	<10	2535	372		43	229	92	5

[a] After resection of pulmonary metastasis of the tumor and chemotherapy.
[b] After high-dose chemotherapy.
[c] After surgical resection of the primary tumor.
[d] AFP, α-fetoprotein.

MSP-SSCP analysis was performed with 15% nondenaturing polyacrylamide gels and silver-staining detection (Daiichi Pure Chemicals). DNA sequencing analysis was performed with a BigDye Terminator Cycle Sequencing FS Ready Reaction Kit and a PRISM 310 Genetic Analyzer (PE Applied Biosystems).

For mutation analysis, all seven exons of the *LDHA* and *LDHB* genes were investigated by PCR-SSCP and DNA sequencing analysis to detect mutations *(9, 10)*. To examine gene amplification, we used two pairs of PCR primers to amplify short fragments of the genomic DNAs of *LDHA* and *LDHB*. These primers, the same ones used for the mutation analysis described above, amplified exon 2 *(9, 10)*. We performed 25, 30, and 35 cycles of PCR and analyzed the *LDHA* and *LDHB* genes separately. PCR products were separated by electrophoresis on 1.5% agarose gels and visualized by ethidium bromide staining and ultraviolet transillumination. Stained bands were analyzed densitometrically with Cool Saver imaging software (ATTO Corp.).

Methylation of the *LDHA* promoter was detected by MSP in three representative tumor regions (1T, 2T, and 3T), with trace bands of unmethylated allele. In the nontumorous region (nontumor control), however, only the unmethylated promoter was observed (Fig. 1A). Products amplified from tumor regions with methylated allele-specific primers showed SSCP patterns similar to the pattern from control methylated DNA with several additional bands or slight smearing. The differences probably originated from partially methylated DNAs that were methylated to various degrees at individual CpG sites. Products amplified from the nontumor control and tumor regions showed the same SSCP pattern as control unmethylated DNA (Fig. 1B). Sequence analysis revealed methylation of CpGs in the *LDHA* promoter region of methylated allele-specific PCR products from tumor regions. No methylation was observed in the unmethylated allele-specific PCR products from the nontumor control region (data not shown).

We did not detect any missense or nonsense mutations in the protein-coding exons and exon-intron boundaries of both the *LDHA* and *LDHB* genes in either the nontumor control or tumor specimens (data not shown). At different cycles of amplification for genomic DNAs of *LDHA* and *LDHB*, the *LDHA*/*LDHB* ratios in the nontumor control samples and the tumor region and the nontumor/tumor ratios in *LDHA* and *LDHB* products did not differ significantly (see Fig. 2 in the online Data Supplement). Therefore, amplification of *LDHB* and deletion of *LDHA* were possibly contradicted.

In mammals, DNA methylation usually occurs at CpG dinucleotides. Methylation is known to play a role in regulation of gene expression during cell development, X chromosome inactivation, genomic imprinting, and carci-

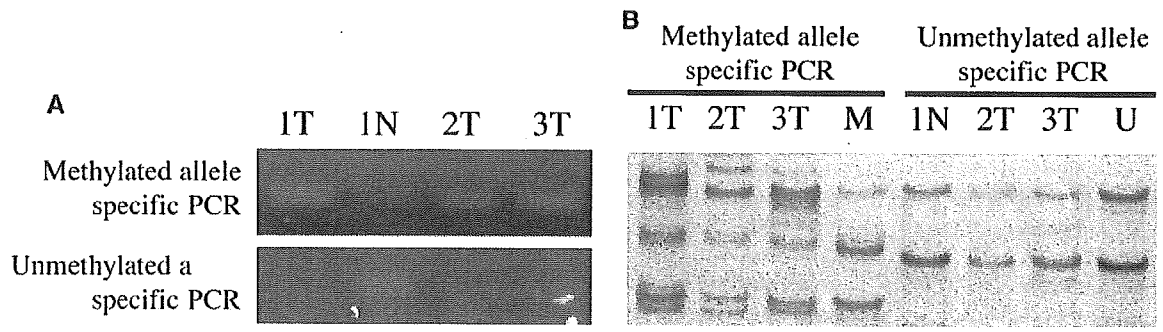

Fig. 1. Methylation analysis.

(*A*), results of bisulfite treatment and MSP analysis of the *LDHA* promoter in three tumor tissue sections (*T*) and one nontumor tissue section (*N*). (*B*), results of SSCP analysis of the above MSP-amplified products. SSCP was performed at 15 °C with 15% polyacrylamide gels. *U*, unmethylated control DNA; *M*, methylated control DNA.

nogenesis (*11, 12*). In neoplastic cells, some usually unmethylated CpG islands in the promoter region become aberrantly methylated, and this leads to transcriptional silencing of various genes (*13*). The human *LDHA* and *LDHB* genes both have CpG-rich regions in their promoters (*14*).

In the patient described here, we observed that the promoter region around exon a of *LDHA* was aberrantly methylated. This might silence expression of the somatic *LDHA* gene, possibly leading to relative increases in LDHB protein concentrations and LD1 activity. We also found that increased concentrations of electrophoretically fast-moving LD isoenzymes in some types of cancer are the result of transcriptional silencing of *LDHA* expression as result of aberrant methylation of the *LDHA* promoter. Thus, as reported previously, enzyme abnormalities in tumors occasionally originate from aberrant methylation. Significant increases in LD1 and LD5 have been reported previously (*15, 16*). The LD isoenzyme patterns in these patients could be the result of aberrant *LDHA* or *LDHB* methylation in cancer cells.

Human testicular germ-cell tumors are typically characterized by overrepresentation of 12p. These tumors were shown to contain striking amplification of a restricted region of 12p that included the K-*ras* protooncogene. Seminomas with this 12p amplification do not undergo apoptosis, and the tumor cells showed prolonged in vitro survival, as do seminoma cells with a mutated *ras* gene (*17*). Indeed, high concentrations of LD1 may yield a better prognostic predictor for the patients with testicular germ cell tumors (*5, 18*). Amplification of 12p is associated with poor prognosis, whereas methylation of *LDHA* may indicate a good prognosis. This issue should be addressed by investigating a large sample of patients with high LD1 attributable to amplification of *LDHB* or methylation of *LDHA*.

To our knowledge, this is the first reported case in which the specific LD isoenzyme pattern in serum was linked directly to promoter methylation. The next issue is whether methylation of the *LDHA* promoter is a common mechanism underlying increased LD1 concentrations in germ-cell tumors.

This research was supported in part by a Health and Labour Sciences Research Grant (H15-9) from the Ministry of Health, Labour and Welfare, Japan; by a Research on Cancer Prevention and Health Services Grant; and by a Grant-in-Aid for Scientific Research (13470518) from the Ministry of Education, Science, Sports, Culture and Technology, Japan.

References

1. Markert CL. Lactate dehydrogenase isozymes: dissociation and recombination of subunits. Science 1963;140:1329–30.
2. Maekawa M. Lactate dehydrogenase isoenzymes. J Chromatogr 1988;429: 373–98.
3. Maekawa M, Inomata M, Sasaki MS, Kenko A, Ushiama M, Sugano K, et al. Electrophoretic variant of lactate dehydrogenase isoenzyme and selective promoter methylation of the *LDHA* gene in a human retinoblastoma cell line. Clin Chem 2002;48:1938–45.
4. Maekawa M, Taniguchi T, Ishikawa J, Sugimura H, Sugano K, Kanno T. Promoter hypermethylation in cancer silences *LDHB*, eliminating lactate dehydrogenase isoenzymes 1–4. Clin Chem 2003;49:1518–20.
5. von Eyben FE. A systematic review of lactate dehydrogenase isoenzyme 1 and germ cell tumors. Clin Biochem 2001;34:441–54.
6. Japanese Society of Clinical Chemistry. Recommendation method for the measurement of human serum enzyme activity–lactate dehydrogenase. Jpn J Clin Chem 2004;33(Suppl):97a–115a.
7. Herman JG, Graff JR, Myohanen S, Nelkin BD, Baylin SB. Methylation-specific PCR: a novel PCR assay for methylation status of CpG islands. Proc Natl Acad Sci U S A 1996;93:9821–6.
8. Maekawa M, Sugano K, Kashiwabara H, Ushiama M, Fujita S, Yoshimori M, et al. DNA methylation analysis using bisulfite treatment and PCR-single-strand conformation polymorphism in colorectal cancer showing microsatellite instability. Biochem Biophys Res Commun 1999;262:671–6.
9. Maekawa M, Sudo K, Kobayashi A, Sugiyama E, Li SS, Kanno T. Fast-type electrophoretic variant of lactate dehydrogenase M(A) and comparison with other missense mutations in lactate dehydrogenase M(A) and H(B) genes. Clin Chem 1994;40:665–8.
10. Sudo K, Maekawa M, Kanno T, Li SS, Akizuki S, Magara T. Premature termination mutations in two patients with deficiency of lactate dehydrogenase H(B) subunit. Clin Chem 1994;40:1567–70.
11. Li E, Beard C, Jaenisch R. Role for DNA methylation in genomic imprinting. Nature 1993;366:362–5.
12. Jones PA. DNA methylation errors and cancer. Cancer Res 1996;56: 2463–7.
13. Baylin SB, Herman JG, Graff JR, Vertino PM, Issa JP. Alterations in DNA methylation: a fundamental aspect of neoplasia. Adv Cancer Res 1998;72: 141–96.
14. Bonny C, Goldberg E. The CpG-rich promoter of human LDH-C is differentially methylated in expressing and nonexpressing tissues. Dev Genet 1995;16: 210–7.
15. Kanowski D, Clague A. Increased lactate dehydrogenase isoenzyme-1 in a case of glucagonoma. Clin Chem 1994;40:158–9.
16. Yamauchi K, Igarashi F, Nakayama T, Yoshida Y, Eto H, Anzai H. A case of gallbladder carcinoma with sustaining high levels of serum lactate dehydrogenase isozyme 1. Jpn J Clin Chem 1991;20:162–7.
17. Roelofs H, Mostert MC, Pompe K, Zafarana G, van Oorschot M, van Gurp RJ, et al. Restricted 12p amplification and RAS mutation in human germ cell tumors of the adult testis. Am J Pathol 2000;157:1155–66.
18. von Eyben FE, de Graaff WE, Marrink J, Blaabjerg O, Sleijfer DT, Koops HS, et al. Serum lactate dehydrogenase isoenzyme 1 activity in patients with testicular germ cell tumors correlates with the total number of copies of the short arm of chromosome 12 in the tumor. Mol Gen Genet 1992;235: 140–6.

Previously published online at DOI: 10.1373/clinchem.2004.037739

Reference Intervals for Serum Calcitonin in Men, Women, and Children, *Jean-Pierre Basuyau,*[1*] *Eric Mallet,*[2] *Marcelle Leroy,*[1] *and Philippe Brunelle*[1] ([1] Laboratoire de Biologie Clinique et de Radioanalyse, Centre Henri-Becquerel, Rouen, France; [2] Service de Pédiatrie, Hôpital Charles-Nicolle, CHU de Rouen, France; * author for correspondence: fax 33-2-32-082590, e-mail jeabas@rouen.fnclcc.fr)

The strategy currently used to investigate thyroid nodules in most cases involves measurement of calcitonin to exclude the possibility of medullary thyroid cancer (MTC). Techniques used to measure calcitonin have become more reliable, sensitive, and easy to perform. Automated nonisotopic techniques now exist, such as the Advantage® system.

We found that some children have particularly high calcitonin. Previous reports also have shown that calcitonin is higher in young children (*1–9*), but most of these studies are now outdated and are based on immunora-

Leukemia (2005), 1–6

www.nature.com/leu

Efficacy of gemtuzumab ozogamicin on ATRA- and arsenic-resistant acute promyelocytic leukemia (APL) cells

A Takeshita[1,2], K Shinjo[1], K Naito[1], H Matsui[1], N Sahara[1], K Shigeno[1], T Horii[2], N Shirai[2], M Maekawa[2], K Ohnishi[1], T Naoe[3] and R Ohno[4]

[1]*Internal Medicine, Hamamatsu University School of Medicine, Hamamatsu, Japan;* [2]*Laboratory Medicine, Hamamatsu University School of Medicine, Hamamatsu, Japan;* [3]*Department of Hematology, Nagoya University, Nagoya, Japan; and* [4]*Aichi Cancer Center, Nagoya, Japan*

Acute promyelocytic leukemia (APL) cells express a considerable level of CD33, which is a target of gemtuzumab ozogamicin (GO), and a significantly lower level of P-glycoprotein (P-gp). In this study, we examined whether GO was effective on all-*trans* retinoic acid (ATRA)- or arsenic trioxide (ATO)-resistant APL cells. Cells used were an APL cell line in which P-gp was undetectable (NB4), ATRA-resistant NB4 (NB4/RA), NB4 and NB4/RA that had been transfected with MDR-1 cDNA (NB4/MDR and NB4/RA/MDR, respectively), ATO-resistant NB4 (NB4/As) and blast cells from eight patients with clinically ATRA-resistant APL including two patients with ATRA- and ATO-resistant APL. The efficacy of GO was analyzed by ^{3}H-thymidine incorporation, the dye exclusion test and cell cycle distribution. GO suppressed the growth of NB4, NB4/RA and NB4/As cells in a dose-dependent manner. GO increased the percentage of hypodiploid cells significantly in NB4, NB4/RA and NB4/As cells, and by a limited degree in NB4/MDR and NB4/RA/MDR cells. Similar results were obtained using blast cells from the patients with APL. GO is effective against ATRA- or ATO-resistant APL cells that do not express P-gp, and the mechanism of resistance to GO is not related to the mechanism of resistance to ATRA or ATO in APL cells.
Leukemia (2005) **0**, 000–000. doi:10.1038/sj.leu.2403807
Keywords: acute promyelocytic leukemia; gemtuzumab ozogamicin (Mylotarg); all-*trans* retinoic acid (ATRA); arsenic trioxide and drug resistance

Introduction

Recently, gemtuzumab ozogamicin (GO, Mylotarg™), a calicheamicin-conjugated humanized anti-CD33 monoclonal antibody (mAb), has been introduced for the treatment of acute myeloid leukemia (AML).[1] However, the clinical outcome after the treatment with GO was negatively associated with P-glycoprotein (P-gp) function in AML.[2] In our previous studies, we found that resistance to GO was mainly mediated by P-gp.[3,4] Acute promyelocytic leukemia (APL) cells express a considerable level of CD33 antigen and a significantly lower level of P-gp compared with other types of AML.[5] Therefore, GO may become established as a successful treatment for APL. In fact, GO has been introduced with the clinical efficacy in the treatment of APL.[6,7] However, *in vitro* efficacy of GO on APL cells as well as all-*trans* retinoic acid (ATRA)- and arsenic trioxide (ATO)-resistant ones has not been studied well. Moreover, drug interaction among ATRA, ATO and GO, and the mechanisms of resistance of APL cells to them remain unclear.[8]

Correspondence: Professor A Takeshita, Laboratory Medicine, Hamamatsu University School of Medicine, 1-20-1 Handayama, Hamamatsu-shi 431-3192, Japan; Fax: +81 53 435 2388;
E-mail: akihirot@hama-med.ac.jp
Received 28 June 2004; accepted 25 March 2005

Materials and methods

Cells

The cell lines used were a human APL cell line, NB4, which was kindly provided by Dr M Lanotte (Hospital Saint-Louis, Paris, France);[9] ATRA-resistant NB4 (NB4/RA) cells; NB4 and NB4/RA cells transfected with MDR-1 cDNA (NB4/MDR and NB4/RA/MDR, respectively); and ATO-resistant NB4 (NB4/As) cells. The NB4/RA and NB4/As cells were obtained by culturing NB4 cells with gradually increasing concentrations of ATRA and ATO, respectively.[10] mdr-1 messenger RNA (mRNA) was not detectable in NB4, NB4/RA or NB4/As cells by RT-PCR.[11,12] NB4/MDR and NB4/RA/MDR cells had detectable mdr-1 mRNA, but did not have detectable MDR-related protein (MRP) mRNA or lung-resistant protein (LRP) mRNA. Blasts were collected from four patients with APL at diagnosis, six patients with clinically ATRA-resistant but ATO-sensitive APL and two patients with clinically ATRA- and ATO-resistant APL.

Flow cytometric analysis for CD33 and Pgp expression

For evaluation of CD33 expression, cells were stained with phycoerythrin (PE)-conjugated anti-CD33 mAb (Becton Dickinson Immuno-cytometry Systems, San Jose, CA, USA), according to the manufacturer's instructions. For P-gp analysis, cells were incubated with biotinylated MRK16 (Fab') mouse mAb or a subclass-matched control mAb, and stained with streptavidine-Per CP (Becton Dickinson Immuno-cytometry Systems) as previously described.[11] Over 10 000 events were analyzed with the Epics XL flow cytometer (Beckman Coulter, Fullerton, CA, USA). APL cells obtained from the patients were also gated by CD-45 staining.[4]

Humanized anti-CD33 mAb and GO

GO consists of three essential parts: an antibody a cytotoxic agent, and a linker. The antibody, humanized IgG4 (hP67.6), targets the CD33 antigen. The cytotoxic agent is *N*-acetyl (NAc)-γ calicheamicin dimethyl hydrazide (DMH), a derivative of calicheamicin antitumor antibiotics.[1,2] GO, humanized non-conjugated anti-CD33 mAb (hP67.6) and free NAc-γ calicheamicin DMH were kindly provided by the Wyeth Research Division of Wyeth Pharmaceuticals Inc. (Philadelphia, PA, USA). The amount of GO used in an experiment was determined based on the concentration of NAc-γ calicheamicin DMH bound to the antibody. One microgram of GO contains 27.1 ng of NAc-γ calicheamicin DMH, and approximately 97% of a GO molecule is composed of the linker and antibody.

Gml : Template: Ver 1.1.3 | Journal: LEU Article : npg_leu_2403807 | ☐ Disk used Pages: 1–6 | Despatch Date: 2/5/2005 Op: vimala Ed:anjana

^{3}H-Thymidine (^{3}H-TdR) incorporation analysis for assessment of cell proliferation

Cells were plated in a 96-well microplate (BD Biosciences, Billerica, MA, USA) at 2×10^5 cells per well in the presence or absence of GO containing 5, 10 or 100 ng/ml NAc-γ calicheamicin DMH or the respective concentration of hP67.6, in 100 μl of RPMI 1640 medium containing 10% fetal calf serum (FCS) and 1 μCi of ^{3}H-TdR. The detailed method was described in our previous papers.[3] The level of ^{3}H-TdR incorporation upon incubation with GO was compared with that upon incubation with hP67.6. The analysis was repeated five times.

Dye exclusion test with propidium iodide staining

After incubation of cells with GO or hP67.6. for the indicated period of time, cells were stained with 0.2 μg/ml propidium iodide (PI) (Sigma, Saint Louis, MO, USA) solution and counted. The numbers of dye-stained (dead) and unstained (living) cells both decreased and the amount of debris rapidly increased, making it difficult to evaluate the cell viability properly. Therefore, viable cells were evaluated. The viable cell count (/ml) after incubation with GO was compared with that after incubation with hP67.6. The analysis was repeated five times.

Cell cycle distributions

The cell cycle distribution was analyzed by flow cytometry with PI staining. The detailed method was described in our previous papers.[3,4] Cell cycle distribution could be analyzed after incubation with 10 or 100 ng/ml of GO for 24 or 48 h. GO temporarily arrests NB4 cells at the G2/M phase, and increases the percentage of hypodiploid cells, by which we evaluated the effect of GO.[3,4] Then, the GO-sensitive cells rapidly change to debris. The analysis was performed in triplicate.

Results

Flow cytometric analysis of CD33 and P-gp expression on NB4 cells and its sublines

The amount of CD33 expressed on the cells did not significantly differ among NB4, NB4/RA, NB4/MDR, NB4/RA/MDR and NB4/As cells. P-gp was not expressed on NB4, NB4/RA or NB4/As cells, in agreement with previous reports.[11,12] Equivalent levels of P-gp were expressed on NB4/MDR and NB4/RA/MDR cells.

^{3}H-TdR incorporation into NB4 cells and its sublines

Upon 72-h incubation with GO containing 5, 10 or 100 ng/ml of NAc-γ calicheamicin DMH, the level of ^{3}H-TdR incorporation into NB4 cells and its sublines decreased in a dose-dependent manner (Figure 1a). In each cell line, the level of ^{3}H-TdR incorporation was lower than that in the same cell line that had been incubated with the corresponding concentration of hP67.6. Upon incubation with GO containing 100 ng/ml NAc-γ calicheamicin DMH, there were significant differences in the level of ^{3}H-TdR incorporation between NB4 and NB4/MDR cells at 48 and 72 h ($P<0.01$ each), and between NB4/RA and NB4/RA/MDR cells at 48 and 72 h ($P<0.01$ each) (Figure 1b). There were no significant differences in the level of ^{3}H-TdR incorporation between NB4 and NB4/RA cells, or between NB4/MDR and NB4/RA/MDR cells at any time point. ^{3}H-TdR incorporation in NB4 cells upon 72-h incubation with GO containing 10 ng/ml NAc-γ calicheamicin DMH corresponded with that with 1000 ng/ml free NAc-γ calicheamicin DMH, which corresponded to a concentration of NAc-γ calicheamicin DMH that was approximately 100 times greater than that in GO. The rate did not change between P-gp-negative and positive NB4 cells.

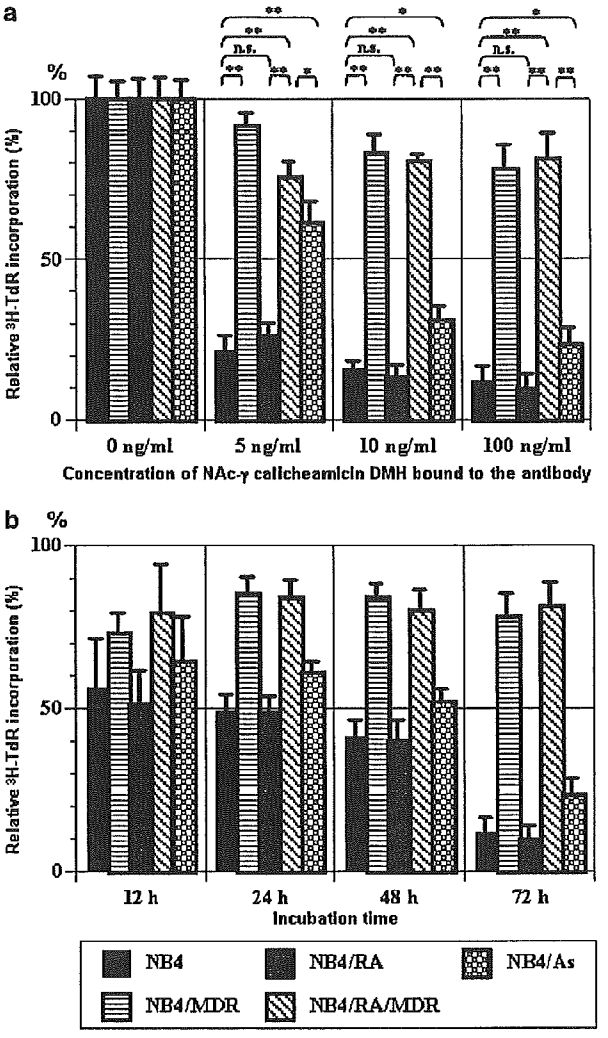

Figure 1 (a) ^{3}H-TdR incorporation by NB4 cells and its sublines after incubation with GO containing 5, 10 or 100 ng/ml NAc-γ calicheamicin DMH or with the respective concentrations of hP67.6 for 72 h. At 72 h, the amount of incorporated ^{3}H-TdR (cpm) was determined by liquid scintillation counting. In (a, b) the amount of incorporated ^{3}H-TdR are expressed as the ratio (%) of incorporated ^{3}H-TdR after incubation with GO to that after incubation with the respective concentration of hP67.6, normalized to 100%. The data from five independent experiments are expressed as mean values of the % response $\pm$ standard deviation (s.d.). At 72 h incubation with hP67.6, the mean level of ^{3}H-TdR incorporation by NB4 cells was 57 000 (53 200–62 300). Statistical significance was calculated by Student's *t*-test. $^*P<0.05$, $^{**}P<0.01$. (b) Time course of ^{3}H-TdR incorporation by NB4 cells and its sublines. Cells were incubated in medium with GO containing 100 ng/ml NAc-γ calicheamicin DMH or the respective concentration of hP67.6 for 12, 24, 48 or 72 h.

Viable cell count analysis by flow cytometry

By the incubation with GO containing 5, 10 or 100 ng/ml of NAc-γ calicheamicin DMH for 72 h, the viable cell counts of NB4 cells and its sublines decreased in a dose-dependent manner (Figure 2a). Figure 2c shows their cell counts upon 24-, 48- or 72-h incubation of these cell lines with GO containing 100 ng/ml NAc-γ calicheamicin DMH or the respective concentration of hP67.6. GO similarly decreased the number of NB4 and NB4/RA cells. GO also decreased the count of NB4/As cells. GO slightly reduced the counts of NB4/MDR and NB4/RA/MDR cells. The counts of NB4 cells and its sublines upon 72-h incubation with GO containing 10 ng/ml NAc-γ calicheamicin DMH corresponded with those with 1000 ng/ml free NAc-γ calicheamicin DMH, respectively.

The combination of ATRA and GO reduced the count of NB4 cells by a greater degree than GO or ATRA alone ($P=0.019$ and $P<0.01$, respectively), but did not reduce the count of NB4/RA cells by a significantly greater degree than GO or ATRA alone (Figure 2b). Upon incubation with GO and ATO, the counts of NB4 and NB4/RA cells were less than those upon incubation with GO ($P<0.01$ each) or ATO alone ($P<0.01$ each).

Cell cycle distribution

The increase percentage in the number of hypodiploid cells on cell cycle distribution upon incubation with GO containing 10 or 100 ng/ml of NAc-γ calicheamicin DMH for 48 h is summarized in Figure 3. The percentage of hypodiploid cells in the NB4, NB4/RA and NB4/As cells was increased upon 12-h incubation with GO, and it was the highest upon 48-h incubation. Beyond 48 h, it was difficult to evaluate the proportion of hypodiploid cells accurately because these GO-sensitive cells transformed into debris, as reported previously (Figure 4).[3] Upon incubation with GO, the percentage of hypodiploid cells in the NB4/MDR and NB4/RA/MDR cells were significantly less than those in the NB4 and NB4/RA cells, respectively ($P<0.01$ each). The addition of ATRA to GO further increased the percentage of hypodiploid cells in NB4 cells ($P=0.043$), but not in NB4/RA cells ($P=0.97$). Upon incubation with GO and ATO, the percentage of hypodiploid cells in NB4 and NB4/RA cells were slightly higher than those upon incubation with GO alone ($P=0.091$ and 0.082, respectively).

Similar results were obtained using blast cells derived from the patients with APL (Table 1). Upon incubation with GO for 48 or 60 h, the hypodiploid portion considerably increased in APL cells that had been obtained from not only the four cases at diagnosis, but also five ATRA-resistant and two ATRA- and ATO-resistant cases. Two patients, whose APL relapsed after achieving complete remission (CR) by ATRA and receiving postremission chemotherapy, were treated according to the Japanese phase 1 and 2 study of GO. They were resistant to re-induction therapy by ATRA, but achieved CR and CR without platelets recovery (CRp) after treatment with GO, respectively.

Discussion

Recently, GO with or without ATRA was introduced for the treatment of APL, and the clinical efficacy of these therapies has been reported in newly diagnosed or relapsed patients with APL.[6,7] There are two basic reasons that support the clinical application of GO on APL. One is that large amounts of CD33 are commonly expressed on the surface of APL cells. Therefore,

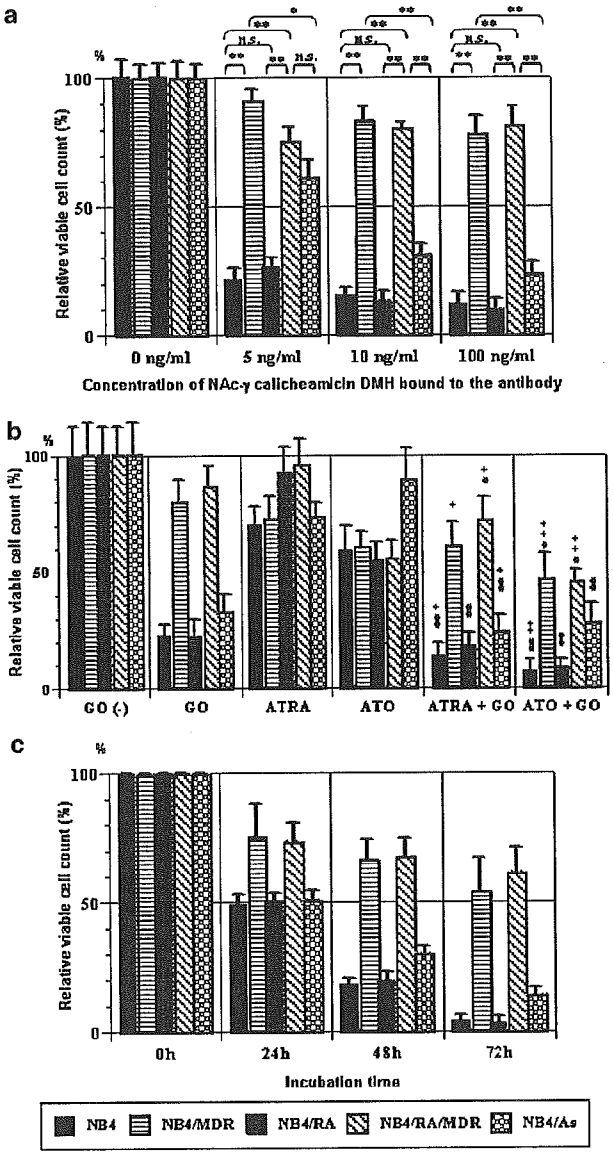

Figure 2 (a) Viable cell counts of NB4 cells and its sublines after incubation with GO containing 5, 10 or 100 ng/ml NAc-γ calicheamicin DMH or with the respective concentrations of hP67.6 for 72 h. The cell counts are expressed as the ratio of the cell counts after incubation with GO to that after incubation with the respective concentration of hP67.6, normalized to 100%. The data from five independent experiments are expressed as mean values of the % count±s.d. Statistical significance was calculated by Student's *t*-test. $^{*}P<0.05$, $^{**}P<0.01$. (b) Viable cell counts of the five cell lines upon incubation with GO containing 5 ng/ml NAc-γ calicheamicin DMH with or without ATRA or ATO for 72 h. The ratio of the cell count after incubation with the agents to that after incubation in the absence of both agents was calculated. Statistical significance was calculated by Student's *t*-test. $^{*}P<0.05$, $^{**}P<0.01$ comparing GO+ATRA or GO+ATO *vs* ATRA alone or ATO alone, respectively. $^{+}P<0.05$, $^{++}P<0.01$ comparing GO+ATRA or GO+ATO *vs* GO alone. (c) Viable cell counts of the five cell lines upon incubation with GO containing 100 ng/ml NAc-γ calicheamicin DMH, or with the respective concentration of hP67.6 for up to 72 h. The ratio (%) of the cell count after incubation with GO to that after incubation with the respective concentration of hP67.6 was calculated.

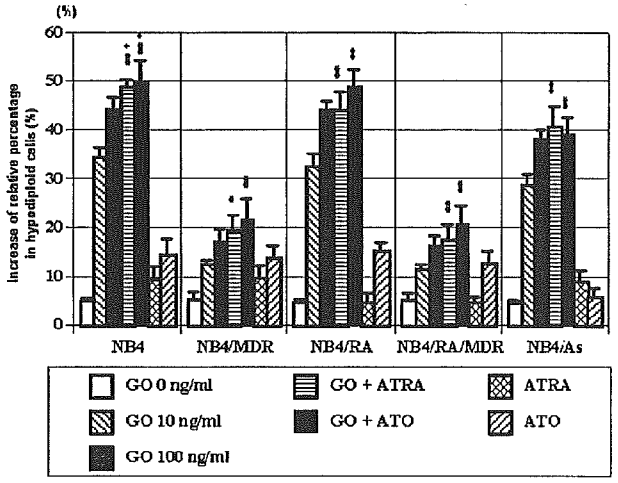

Figure 3 Percentage of hypodiploid cells in cell cycle distribution patterns upon 48-h incubation with GO containing 10 or 100 ng/ml of NAc-γ calicheamicin DMH or with the respective concentrations of hP67.6. Cells were also incubated with GO containing 100 ng/ml of NAc-γ calicheamicin DMH in combination with 10^{-6} M ATRA or 10^{-6} M ATO. Each bar represents the mean ± s.d. of three experiments. *$P<0.05$, **$P<0.01$ comparing GO + ATRA or GO + ATO *vs* ATRA alone or ATO alone, respectively. $^{+}P<0.05$, $^{++}P<0.01$ comparing GO + ATRA or GO + ATO *vs* GO alone.

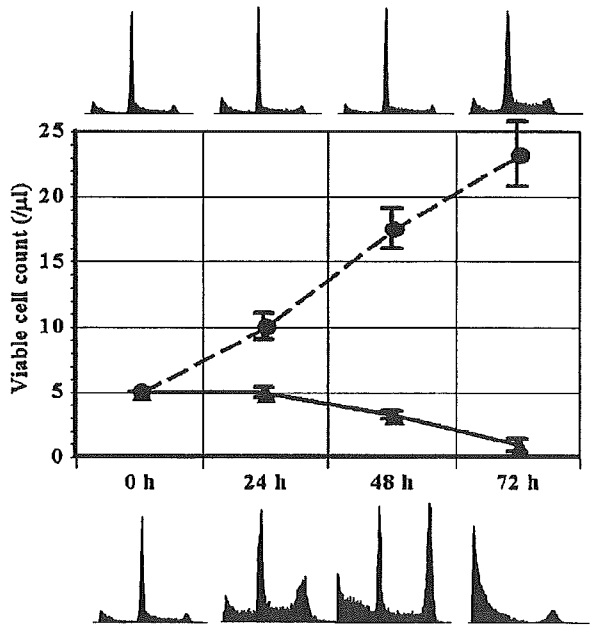

Figure 4 The cell growth curve and cell cycle distributions of NB4 cells upon 24-, 48- and 72-h incubation with GO containing 10 ng/ml NAc-γ calicheamicin DMH (continuous line and lower distribution patterns, respectively) or with the respective concentrations of hP67.6 (dotted line and upper distribution patterns, respectively).

several different anti-CD33 mAbs have been used for the treatment of APL, and notable results have been reported, especially in the use of GO.[6,7] Another reason is that a low level of P-gp is expressed on APL cells.[5] GO is sometimes not effective in some other subtypes of AML because the detached calicheamicin derivative is pumped out by P-gp.[3,4] Therefore, this mechanism of resistance to GO is not theoretically applicable to APL cells.

In this study, GO showed antiproliferative and cytocidal effects on ATRA-resistant NB4 cells as well as NB4 cells. We previously demonstrated that MDR modifiers, PSC833 and MS209, had no effect on ATRA-resistance in APL, which indicated that P-gp has a limited role in ATRA-resistance.[11] Intracellular ATRA concentration was not influenced by P-gp.[11] Clinical evidence, including our reports, also supported the independence of P-gp and ATRA-resistance.[13] Taking these data into consideration, GO is predictably effective on ATRA-resistant APL unless P-gp is expressed.

In the previous report, the combination of GO and ATRA was given to some patients with APL. In a study conducted in the US, GO was administered with ATRA to 19 patients with untreated APL.[6] The CR rate was 16/19 (84%), and 14 became PCR-negative. In relapsed APL, Lo-Coco *et al*[7] reported 14 cases of patients who achieved molecular remission after treatment with GO among 16 relapsed APL cases. However, there has been no *in vitro* study to explain these clinical efficacies. We performed the present study using NB4 and its drug-resistant sublines in an attempt to elucidate the mechanisms of GO. In APL, the drug resistance, which has been studied and discussed previously, might be built up by multiple causes and procedures.[8,13] Further studies on APL should be performed from many directions. It is also important to determine the optimal dosage of these drugs as well as the optimal timing of their administration.

GO also showed efficacy on ATO resistant NB4 cells, which do not express P-gp. The cellular glutathione and MRP levels are reported with their relationship to ATOresistance.[10,14] Walter *et al*[15] reported that MRP1 might attenuate the susceptibility to GO, although by a smaller degree than P-gp. We could not find an obvious relationship between MRP1 and GO resistance.[16] Our data suggest that the MRP and the cellular glutathione levels play limited roles, while P-gp plays a major role in GO resistance.

GO showed antiproliferative and cytocidal effects on APLs that do not express P-gp (Figure 4). GO increased the percentage of hypodiploid cells (Figure 3) while it inhibited cell proliferation in the early phase (Figures 1 and 2). After undergoing these changes, GO-sensitive cells rapidly collapsed into debris. The time-lag and variation of the effect of GO on APL cells might be explained by differences in the level of CD33 expression on the cells, and the length of time required for binding, and internalization of GO and detachment of calicheamicin from GO. Alternatively, GO could have various different actions against cells. Apoptosis, which is one of the main mechanisms of GO, did not explain all of the observed morphological changes of GO-treated cells in our previous study using videomicroscopy.[3] However, analysis of the changes in cell cycle distribution could be a valuable test for analyzing the susceptibility of AML cells to GO. It has a high degree of usability for samples derived from cases that contain different phenotypes.

We confirmed the antileukemia effect of GO on APL in an *in vitro* study using an APL cell line and its ATRA- and ATO-resistant sublines. GO seems to be promising for the treatment of not only untreated but also relapsed APL. A larger clinical study of GO for the treatment of relapsed and refractory APL is needed. The results of such study may suggest how GO should be integrated into the management of APL.

Table 1 Background of the patients and *in vitro* effect of GO on the cell cycle

Case no.	Sex	Age (year)	t(15;17)[a]	PML/RARα[b]	Status	Blast (%) in bone marrow	CD33 (%)	P-gp (%)	% increase in hypodiploid cells by GO[c]		Clinical response to ATRA	Clinical response to ATO	Clinical response to GO
									48 h	60 h			
DIAG-1	M	63	(+)	(+)	At diagnosis	92.2	99	3.7	13.2	22.7	CR	NT	NT
DIAG-2	F	21	(+)	(+)	At diagnosis	88.0	97.9	1.8	17.5	25.3	CR	NT	NT
DIAG-3	M	55	(+)	(+)	At diagnosis	67.6	97.8	3.5	12.1	17.9	CR	NT	NT
DIAG-4	M	51	(+)	(+)	At diagnosis	68.1	88.3	4.1	18.3	35.8	CR	NT	NT
ATRA-1	F	36	(+)	(+)	2nd relapse	20.2	98.7	1.8	10.7	18.4	NR	CR	NT
ATRA-2	M	57	(+)	(+)	2nd relapse	83.2	89.8	9.1	6.6	8.1	NR	CR	NT
ATRA-3	F	38	(+)	(+)	2nd relapse	77.2	94.6	1.4	16.9	27.9	NR	CR	NT
ATRA-4	F	21	(+)	(+)	2nd relapse	94.8	97.8	0.1	32.4	43.5	NR	CR	NT
ATRA-5	M	51	(−)	(+)	3rd relapse	30.8	97.9	4.4	9.6	12.8	NR	NT	CR
ATRA-6	M	48	(+)	(+)	3rd relapse	86.0	97.1	4.2	13.8	25.6	NR	NT	CRp
ATO-1	M	50	(+)	(+)	3rd relapse	78.0	83.6	11.6	10.8	13.4	NR	NR	NT
ATO-2	F	38	(+)	(+)	2nd relapse	38.7	85.4	4.5	9.5	15.3	NR	NR	NT

[a]Karyotype was analyzed by G-banding.
[b]PML/RARα was analyzed by RT-PCR or FISH.
[c]Defined as the difference in the percentage of hypodiploid cells between samples that had been incubated with nonconjugated anti-CD33 mAb or GO.
NT, not treated by ATO or GO *in vivo*; NR, no response; CR, complete remission; CRp, CR without platelets recovery.
After treatment with GO, the percentage of hypodiploid cells considerably increased in APL cells that had been obtained not only from the four patients at diagnosis but also from several ATRA-resistant patients and ATRA-and-ATO-resistant patients. Two patients, whose APL relapsed after achieving CR by ATRA and receiving postremission chemotherapy, were treated according to the Japanese phase 1 or 2 study of GO. They were resistant to reinduction therapy by ATRA, but achieved CR and CRp by treatment with GO, respectively. The coefficient of correlation (r) between the percentage of P-gp expression and the increase in hypodiploid portion was 0.60 and 0.65 upon 48- and 60-h incubation with GO, respectively.

Acknowledgements

We express our sincere gratitude to Ms Satoko Kanomi (Wyeth Pharmaceuticals Inc.) for continuous support, and to Ms Yoshimi Suzuki, Ms Noriko Anma and Dr Kiyoshi Shibata (Equipment Centre at Hamamatsu University School of Medicine) for technical assistance. This study was supported by Japanese grants-in-aid from the Ministry of Health and Welfare (No. 9-2) and the Ministry of Education and Science (No. 14570972).

References

1 Sievers EL, Larson RA, Stadtmauer EA, Estey E, Lowenberg B, Dombret H, *et al.*, Mylotarg Study Group. Efficacy and safety of gemtuzumab ozogamicin in patients with CD33-positive acute myeloid leukemia in first relapse. *J Clin Oncol* 2001; **19**: 3244–3254.
2 Linenberger ML, Hong T, Flowers D, Sievers EL, Gooley TA, Bennett JM *et al.* Multidrug-resistance phenotype and clinical responses to gemtuzumab ozogamicin. *Blood* 2001; **98**: 988–994.
3 Naito K, Takeshita A, Shigeno K, Nakamura S, Fujisawa S, Shinjo K *et al.* Calicheamicin-conjugated humanized anti-CD33 monoclonal antibody (gemtuzumab zogamicin, CMA-676) shows cytocidal effect on CD33-positive leukemia cell lines, but is inactive on P-glycoprotein-expressing sublines. *Leukemia* 2000; **14**: 1436–1443.
4 Matsui H, Takeshita A, Naito K, Shinjo K, Shigeno K, Maekawa M *et al.* Reduced effect of gemtuzumab ozogamicin (CMA-676) on P-glycoprotein and/or CD34-positive leukemia cells and its restoration by multidrug resistance modifiers. *Leukemia* 2002; **16**: 813–819.
5 Paietta E, Andersen J, Racevskis J, Gallagher R, Bennett J, Yunis J *et al.* Significantly lower P-glycoprotein expression in acute promyelocytic leukemia than in other types of acute myeloid leukemia: immunological, molecular and functional analyses. *Leukemia* 1994; **8**: 968–973.
6 Estey EH, Giles FJ, Beran M, O'Brien S, Pierce SA, Faderl SH *et al.* Experience with gemtuzumab ozogamycin ('mylotarg') and all-*trans* retinoic acid in untreated acute promyelocytic leukemia. *Blood* 2002; **99**: 4222–4224.
7 Lo-Coco F, Cimino G, Breccia M, Noguera NI, Diverio D, Finolezzi E *et al.* Gemtuzumab ozogamicin (Mylotarg) as a single agent for molecularly relapsed acute promyelocytic leukemia. *Blood* 2004; **104**: 1995–1999.
8 Gallaher RE. Retinoic acid resistance in acute promyelocytic leukemia. *Leukemia* 2002; **16**: 1940–1958.
9 Rybner C, Hillion J, Sahraoui T, Lanotte M, Botti J. All-*trans* retinoic acid down-regulates prion protein expression independently of granulocyte maturation. *Leukemia* 2002; **16**: 940–948.
10 Kitamura K, Minami Y, Yamamoto K, Akao Y, Kiyoi H, Saito H *et al.* Involvement of CD95-independent caspase 8 activation in arsenic trioxide-induced apoptosis. *Leukemia* 2000; **14**: 1743–1750.
11 Takeshita A, Shinjo K, Naito K, Ohnishi K, Sugimoto Y, Yamakawa Y *et al.* Role of P-glycoprotein in all-*trans* retinoic acid (ATRA) resistance in acute promyelocytic leukaemia cells: analysis of intracellular concentration of ATRA. *Br J Haematol* 2000; **108**: 90–92.

12 Takeshita A, Shinjo K, Naito K, Matsui H, Shigeno K, Nakamura S *et al*. P-glycoprotein (P-gp) and multidrug resistance-associated protein 1 (MRP1) are induced by arsenic trioxide (As(2)O(3)), but are not the main mechanism of As(2)O(3)-resistance in acute promyelocytic leukemia cells. *Leukemia* 2003; **17**: 648–650.
13 Ohno R, Asou N, Ohnishi K. Treatment of acute promyelocytic leukemia: strategy toward further increase of cure rate. *Leukemia* 2003; **17**: 1454–1463.
14 Yang C-H, Kuo M-L, Chen J-C, Chen Y-C. Arsenic trioxide sensitivity is associated with low level of glutathione in cancer cells. *Br J Cancer* 1999; **81**: 796–799.
15 Walter RB, Raden BW, Hong TC, Flowers DA, Bernstein ID, Linenberger ML. Multidrug resistance protein attenuates gemtuzumab ozogamicin-induced cytotoxicity in acute myeloid leukemia cells. *Blood* 2003; **102**: 1466–1473.
16 Naito K, Takeshita A, Matsui H, Horii T, Maekawa M, Kitamura K *et al*. Multidrug resistance (MDR)-related protein 1 (MRP1) and lung resistance protein (LRP) are not the main drug resistance mechanisms of gemtuzumab ozogamicin (CMA-676) in AML. *Hematol J* 2002; **3**: 1048a.

Clinical Chemistry 50:8
1322–1327 (2004)

Molecular Diagnostics and Genetics

Three-Dimensional Microarray Compared with PCR–Single-Strand Conformation Polymorphism Analysis/DNA Sequencing for Mutation Analysis of K-*ras* Codons 12 and 13

MASATO MAEKAWA,[1*] TOMONORI NAGAOKA,[1,3] TERUMI TANIGUCHI,[1] HITOMI HIGASHI,[1] HARUHIKO SUGIMURA,[2] KOKICHI SUGANO,[4] HIROYUKI YONEKAWA,[5] TAKATOMO SATOH,[3] TOSHINOBU HORII,[1] NAOHITO SHIRAI,[1] AKIHIRO TAKESHITA,[1] and TAKASHI KANNO[1]

Background: We developed a rapid, precise, and accurate microarray-based method that uses a three-dimensional platform for detection of mutations.

Methods: We used the PamChip® microarray to detect mutations in codons 12 and 13 of K-*ras* in 15 cell lines and 81 gastric or colorectal cancer tissues. Fluorescein isothiocyanate-labeled PCR products were analyzed with the microarray. We confirmed the microarray results with PCR–single-strand conformation polymorphism (SSCP) analysis and DNA sequencing.

Results: We could correctly identify wild-type, heterozygous, and homozygous mutant genotypes with the PamChip microarray in <3.5 h. The array data were consistent with those of PCR-SSCP analysis and DNA sequencing. All 15 cell lines and 80 of 81 clinical cancer specimens (98.8%; 95% confidence interval, 96.4–100%) were genotyped accurately with the microarray, a rate better than that of direct DNA sequencing (38.9%) or SSCP (93.8%). Only one clinical specimen was misdiagnosed as homozygous for the wild-type allele. Densitometric analysis of SSCP bands indicated that the content of the mutant allele in the specimen was ~16%. The PamChip microarray could detect mutant alleles representing more than 25% of the SSCP band proportions. Therefore, the limit for detection of mutant alleles by the PamChip microarray was estimated to be 16–25% of the total DNA.

Conclusions: The PamChip microarray is a novel three-dimensional microarray system and can be used to analyze K-*ras* mutations quickly and accurately. The mutation detection rate was nearly 100% and was similar to that of PCR-SSCP together with sequencing analysis, but the microarray analysis was faster and easier.

Microarray technologies were initially developed to study differential gene expression in complex populations of RNA in tissues. Microarrays used for such purposes have a high density of spots (*1*, *2*). Detection of single-nucleotide polymorphisms (SNPs) by microarrays is a versatile methodology that is suitable for high-throughput diagnostic procedures (*3*, *4*). SNP detection and genotyping have also been done by PCR–single-strand conformation polymorphism (PCR-SSCP) analysis, degenerate HPLC, PCR–restriction fragment length polymorphism analysis, DNA sequencing, TaqMan PCR, and the Invader assay (*5*). DNA microarrays have also been used for genotyping applications, including SNP typing, detection of genomic and somatic mutations, identification of microbes, and detection of allelic imbalances (*6–11*). Commercially available microarrays have features beyond simple passive hybridization, including microfabricated fluidic channels, electronic hybridization, novel posthybridization signaling steps, and flow-through dynamics (*12*, *13*).

Recently, PamGene International B.V. developed a novel three-dimensional flow-through platform that uses a porous aluminum oxide substrate as a solid support (*14*). Because the substrate has long branched capillaries,

[1] Department of Laboratory Medicine and [2] 1st Department of Pathology, Hamamatsu University School of Medicine, Hamamatsu, Japan.
[3] Genome Medical Business Division, OLYMPUS Corporation, Hachioji, Japan.,
[4] Oncogene Research Unit/Cancer Prevention Unit, Tochigi Cancer Center Research Institute, Utsunomiya, Japan.
[5] Scientific Equipment Group, OLYMPUS America, Inc., New York, NY.
*Address correspondence to this author at: Department of Laboratory Medicine, Hamamatsu University School of Medicine, Hamamatsu 431-3192, Japan. Fax 81-53-435-2794; e-mail mmaekawa@hama-med.ac.jp.
Received January 28, 2004; accepted May 17, 2004.
Previously published online at DOI: 10.1373/clinchem.2004.032060

the reactive surface of this material is several-hundred-fold greater than that of a two-dimensional surface. Therefore, the flow-through microarray reduces hybridization times and increases signal and signal-to-noise ratios. This unique platform technology has been used by PamGene International B.V. and OLYMPUS Corporation to develop the PamChip® microarray and FD10 microarray system. The PamChip microarray has a disposable housing optimized for flow-through hybridization of samples. The hybridization is performed by repeated pumping of the sample solution up and down through the substrate. FD10 is an integrated PamChip microarray system that has solution-driven incubation and image acquisition functions with the ability to analyze and process four arrays simultaneously as well as optimized software for analysis. This system has already been used for gene expression profiling *(15)*.

K-*ras* is an oncogene in which various point mutations are frequently detected in cancers of the digestive organs. The mutations are clustered in a very narrow region, codons 12 and 13 *(16)*. The mutation sites in codon 12 are considered a mutational hot spot in carcinogenesis, which makes K-*ras* a promising candidate for mutation screening with microarray technologies.

Here we describe a rapid, precise, and accurate microarray system that uses the three-dimensional platform technology for mutation detection. Retrospective and/or comparative analyses were performed for mutations in codons 12 and 13 of K-*ras*.

Materials and Methods

SAMPLES AND DNA ISOLATION

Cancer cell lines were obtained from the Japanese Cell Resource Bank (COLO320, MKN1, MKN7, MKN28, MKN45, MKN74, KATOIII, A431, and LU65) and from the American Type Culture Collection (SW1116). The NEDATE cell line was established at the National Cancer Center Hospital. The C-1 and PSN1 cell lines were kindly supplied by the Pathology Division of the National Cancer Center Research Institute. Lymphoblastoid cell lines (TK6 and WTK-1) were obtained from the National Institute of Health Science. Genomic DNA was extracted from 15 cell lines as described previously *(17, 18)*.

DNA samples extracted from gastric or colorectal cancer tissues and corresponding healthy mucosae were selected from DNA stocks at Hamamatsu University School of Medicine, National Cancer Center Hospital, and Tochigi Cancer Center Hospital by K-*ras* mutation typing based on previously performed PCR-SSCP analysis. The experimental design was approved by the Committee for Genetic Analysis at Hamamatsu University School of Medicine.

PCR-SSCP ANALYSIS AND DIRECT SEQUENCING

The PCR primers used have been described previously *(19)*. These primers amplify a 108-bp fragment containing codons 12 and 13. PCR was performed with *Ex*Taq (TaKaRa), and the amplified products were sequenced directly or subjected to SSCP analysis on 10% nondenaturing polyacrylamide gels (Daiichi Pure Chemicals) *(20)*. Occasionally, extra bands (possibly mutated) detected by SSCP were excised from gels, reamplified, and sequenced. PCR products showing mobility shifts were then sequenced directly with the BigDye Terminator Cycle Sequencing FS Ready Reaction Kit and ABI PRISM 310 Genetic Analyzer (Applied Biosystems).

MICROARRAY ANALYSIS

Oligonucleotide probes (17mers) were designed to detect K-*ras* mutations (see Table 1 in the Data Supplement that accompanies the online version of this article at http://www.clinchem.org/content/vol50/issue8/) and spotted on PamChip microarrays. The layout of the PamChip microarrays is shown in Fig. 1. Wild-type probes for codons 12 and 13 (GGTGGC; shaded circles in Fig. 1) and eight mutations (CGTGGC, TGTGGC, AGTGGC, GCTGGC, GATGGC, GTTGGC, GGTGAC, and GGTTGC, where the underlined bases are the sites of the mutations; open and hatched circles in Fig. 1) were used for hybridization.

A mixture of 5′-fluorescein isothiocyanate-labeled oligonucleotides complementary to the wild-type (GGTGGC) and mutant (GATGGC, CGTGGC, and AGTGGC) sequences were used as hybridization probes in a standard dilution mixture series. The ratios of wild type to mutant (in μmol/L) in the mixtures were 0:10, 2:8, 4:6, 6:4, 8:2, and 10:0. In addition, mixtures of genomic DNA prepared from cell lines were amplified and then subjected to the microarray analysis.

Before hybridization, the test site of each array was washed with 1 mL/L Tween 20 for one pumping cycle. Amplification products (108 bp) were generated with 5′-fluorescein isothiocyanate-labeled primers, denatured for 3 min at 94 °C, and cooled to 4 °C on ice. The target DNA, which was 10 μL of either denatured PCR product or oligonucleotide mixture, was mixed with 40 μL of 1.25× standard saline phosphate–EDTA in the well of a PamChip microarray preheated to 55 °C, and the hybridization was started immediately in the FD10 system. In this flow-through hybridization analysis, the liquid flow

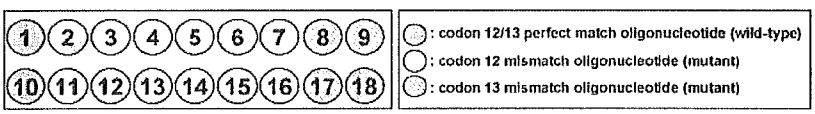

Fig. 1. PamChip microarray layout.

Wild-type (*shaded circles*) and/or mutant (*open* and *hatched circles*) probes were used for hybridization. *Numbers* correspond to those in Table 1 of the online Data Supplement (available at http://www.clinchem.org/content/vol50/issue8/).

rate was 10 μL/s. After 30 cycles (~10 min) of flow-through hybridization at 55 °C, each array was washed once with 1× standard saline phosphate–EDTA with pumping. Array images were captured automatically on the FD10 system and then analyzed with the integrated image acquisition and analysis software.

Results

To examine assay reproducibility and accuracy, we used three PamChip microarrays, each of which contained four test channels. Mixtures of oligonucleotides complementary to wild-type and mutant-type probes were hybridized to the PamChip microarray in duplicate. Signal intensities were not always consistent with the theoretical mixture ratio, however, because there were dose–response effects in each mixture. Representative results obtained with the different ratios of the mixture of GGTGGC (wild type) and GATGGC (mutant) are shown in Fig. 2A. In addition, we used mixtures of genomic DNA prepared from cell lines in the different ratios. Representative results obtained with the mixture of MKN45 (wild-type; GGTGGC) and Lu65 (mutant; TGTGGC) are shown in Fig. 2B.

We tested both sense and antisense strands as hybridization probes. In general, the sense strand identified genotypes more accurately. Results of the PamChip microarray analysis of a homozygous wild-type specimen (GGTGGC) with sense and antisense oligonucleotides as hybridization probes are shown in Fig. 3. A single strong signal for GGTGGC was observed when the sense strand was used as a probe, whereas weak, noisy signals were observed with the antisense probes. We therefore used the sense strand probe in further analyses.

Wild-type, heterozygous, and homozygous mutant genotypes were detected accurately and reliably in 15 cell lines with the PamChip microarray in a relatively short

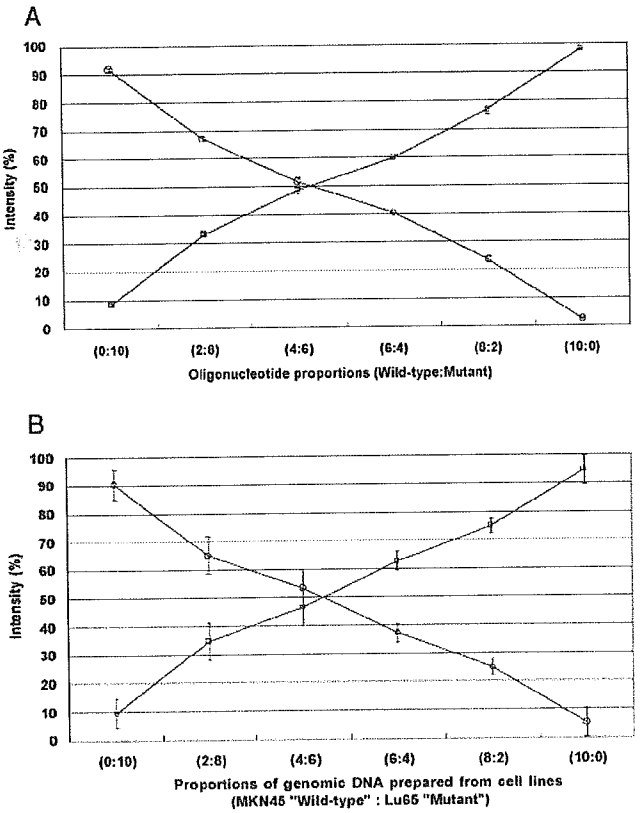

Fig. 2. Fluorescence intensities obtained with complementary oligonucleotides (*A*) and genomic DNA (*B*).

(*A*), relationship between hybridization signal intensity and oligonucleotide population ratio. The fluorescence intensities of hybridization signals were examined with use of the complementary oligonucleotides GGTGGC and GATGGC. The relative fluorescence intensities in mixtures consisting of GGTGGC (□) and GATGGC (○) were calculated by the following formulas: GGTGGC (%) = GGTGGC signal intensity/(GGTGGC signal intensity + GATGGC signal intensity) × 100; and GATGGC (%) = GATGGC signal intensity/(GGTGGC signal intensity + GATGGC signal intensity) × 100. (*B*), representative results obtained with the mixture of genomic DNA prepared from two cell lines, MKN45 (wild-type; GGTGGC) and Lu65 (mutant; TGTGGC). The fluorescence intensities were calculated as described above. □, wild-type intensities; ○ mutant intensities. Each *symbol* represents the mean of four independent microarray results (*error bars*, SD).

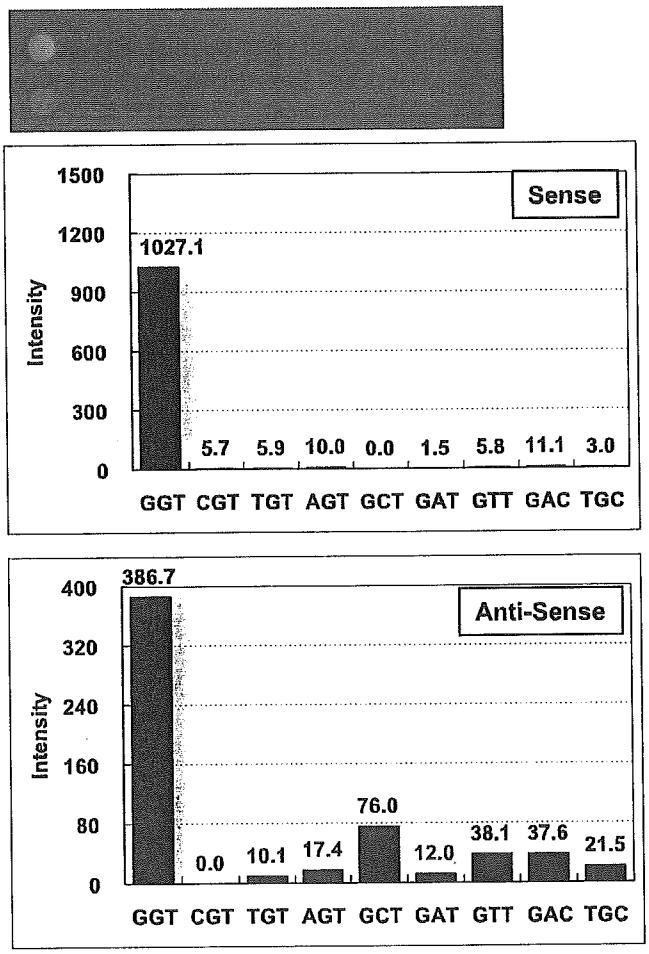

Fig. 3. Comparison of sense and antisense strands as hybridization probes.

Hybridization images in the *top* and *bottom rows* in the *array* (*top*) represent the results obtained with the sense and antisense strands, respectively, used as hybridization probes. The subsequent data analyses (*middle* and *bottom*) show the comparison quantitatively.

time. All results correlated with those of PCR-SSCP analysis and DNA sequencing. DNAs from clinical specimens were also analyzed with the PamChip microarray for comparison with PCR-SSCP analysis and/or DNA sequencing. Fig. 4 shows examples of images captured on the FD10 system and results of subsequent data analyses. Essentially, the results obtained with the PamChip microarray were consistent with those of PCR-SSCP analysis and DNA sequencing. Eighty-one clinical cancer specimens were analyzed with the PamChip microarrays, and the genotypes of 80 of these specimens (98.8%) were identified accurately. PCR-SSCP analysis detected all 64 samples homozygous or heterozygous for mutant genotypes in codon 12. The remaining 17 (of 81) specimens were homozygous or heterozygous for mutant alleles in codon 13, but they could not be identified by SSCP analysis because mutant alleles in codon 13 were not used as a reference for SSCP. Although SSCP bands in 12 of the 17 samples were clearly different from those of the wild-type alleles, the remaining 5 samples were misclassified into the mutant genotype, GATGGC, because of the similar electrophoretic pattern. Therefore, the distinct misidentification was 5, and genotyping succeeded in 76 of 81 samples (93.8%). Thirty-six samples (10 homozygous and 26 heterozygous mutant genotypes) were analyzed by direct DNA sequencing. The 10 samples homozygous for mutant genotypes were identified properly. Twenty-two of the 26 heterozygous mutant samples were misclassified into homozygous wild type, and only the remaining 4 samples were correctly identified. In total, 14 of 36 samples (38.9%) were diagnosed accurately.

Only one sample, a clinical specimen from a patient with colorectal cancer, was classified incorrectly by the PamChip microarray. PamChip analysis yielded a homozygous wild-type genotype, whereas SSCP analysis and DNA sequencing indicated that the genotype was GGTGGC/GATGGC. The semiquantitative proportions obtained by densitometric analysis of SSCP bands were then compared with PamChip microarray and direct DNA sequencing data. The results for clinical specimens are shown in Table 2 of the online Data Supplement. The samples were heterozygous for wild-type and mutant alleles in various proportions. In the single misdiagnosed clinical specimen, the content of the mutant allele was

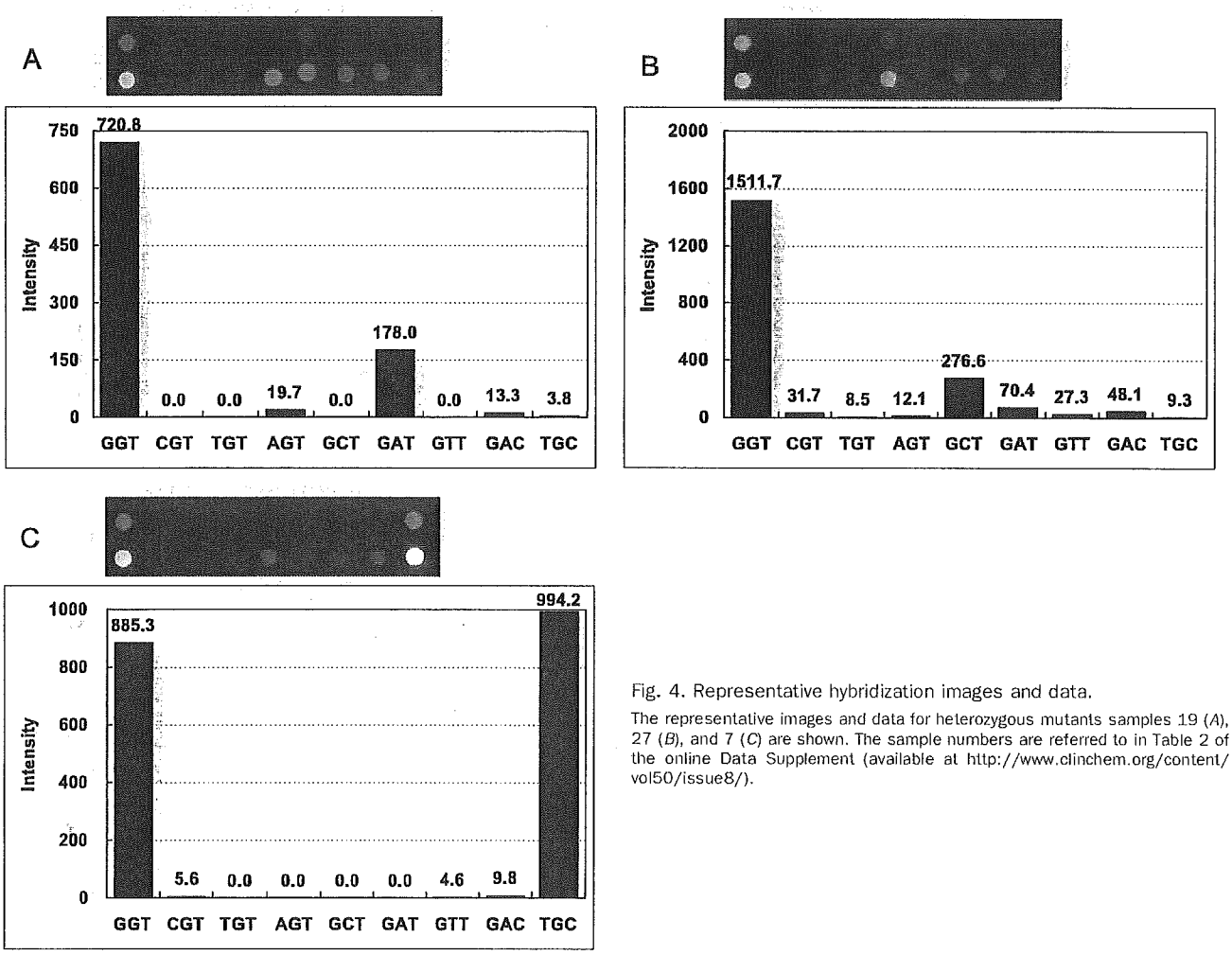

Fig. 4. Representative hybridization images and data.

The representative images and data for heterozygous mutants samples 19 (*A*), 27 (*B*), and 7 (*C*) are shown. The sample numbers are referred to in Table 2 of the online Data Supplement (available at http://www.clinchem.org/content/vol50/issue8/).

estimated to be ~16% by SSCP analysis. The PamChip microarray could detect mutant alleles proportions >25% by SSCP analysis. The limit for detection of mutant alleles by the PamChip microarray was therefore estimated to be 16–25% of the total DNA. The detection limit of direct sequencing was estimated to be 46–50%.

Discussion

In this study, we analyzed several mixtures containing two oligonucleotides (wild-type plus mutant) with the PamChip microarray. We also analyzed mixtures of genomic DNA (wild-type and mutant) prepared from two cell lines with the PamChip microarray. The fluorescence intensities of each sequence showed dose-dependent relationships and were somewhat consistent with the theoretical proportions in the mixtures of genomic DNA as well as oligonucleotides. Such results for microarray analysis have not been described previously. The accuracy of the fluorescence intensity and the degree of fluorescence were satisfactory and are suitable for microarray analysis.

Clinical DNA samples were analyzed with the PamChip microarray for comparison with PCR-SSCP analysis and/or DNA sequencing data. When somatic mutations in cancer tissues are assessed, it is not possible to avoid contamination by the wild-type allele derived from noncancer cells. We therefore investigated the limit at which each technique could detect the mutant allele. The ability to detect small amounts of mutant DNA within a large amount of wild-type DNA is absolutely necessary for analyzing clinical DNA samples. The combination of PCR-SSCP analysis and DNA sequencing provided the greatest sensitivity. Direct sequencing of PCR products occasionally misdiagnosed samples containing low amounts of the mutant allele (46–50%), and PCR-SSCP analysis could not distinguish genotypes with similar electrophoretic patterns. The PamChip microarray detected DNA mutations when the mutation comprised at least 25% of the tested population of DNA; thus, we believe that samples from patients heterozygous for a particular mutation, i.e., cancer specimens contaminated with noncancerous tissue, would be detectable with this array system. Mutations in mitochondrial DNAs that cause disease typically occur as mixtures of mutant and wild-type mitochondrial DNAs (heteroplasmy), and disease severity is correlated with the proportion of mutant DNA (*21*). Genotyping of mitochondrial DNA mutations in such diseases can also be performed with this array system.

The entire PamChip process was completed in ~3.25 h, including 1 h for DNA preparation, 2 h for PCR, and 15 min for microarray (hybridization, washing, and signal detection). The PamChip microarray thus substantially reduces the time necessary for microarray analysis. However, at present the PamChip microarray requires PCR amplification of the targeted region, which adds 2–3 h to the total analysis time. To reduce the time for DNA amplification, shuttle PCR or another amplification method may be useful. Multiplex PCR can be used to amplify multiple SNPs simultaneously. A novel microarray analysis that does not require DNA amplification or preparation would be superior for mutation and/or SNP analysis. Such a technique could be easily applied to the selection of medications best suited for each individual and to molecular diagnosis during surgery.

K-*ras* mutations are typically localized in codons 12, 13, and 61, and ~60% of somatic mutations in cancers occur in codon 12. Amino acid substitutions may affect the physiologic function of a protein and the clinical prognosis. A close association has been reported between a somatic mutation, GAT (Asp), in codon 12 and distant hematogenous metastasis (*22*). Two specific mutations, TGT (Cys) in codon 12 and GAC (Asp) in codon 13, have been associated with a significantly increased risk of cancer recurrence (*23*). Etiologic data revealed that GTT (Val) in codon 12 is associated with cancer progression and more aggressive biological behavior (*24*, *25*). Consequently, genotyping of colorectal adenocarcinomas for K-*ras* status is feasible for use in diagnostic pathology to provide information that could be used to individualize and optimize treatments and prognoses.

In conclusion, the unique features of the PamChip microarray technology, including real-time imaging and temperature control combined with short assay time, make it suitable for clinical screening of mutations. This microarray is potentially useful for limited and targeted purposes, and detection of K-*ras* mutations is one example of such focused use of this microarray.

This research was supported in part by a Grant-in-Aid for Labour Sciences Research (H15-Cancer Prevention-9) for research on cancer prevention and health services; by a Grant-in-Aid from the Second Term Comprehensive 10-Year Strategy for Cancer Control from the Ministry of Health, Labour and Welfare, Japan; by a Grant-in-Aid for Scientific Research (B), for COE (Hamamatsu University School of Medicine); by a Grant-in-Aid from the Ministry of Education, Science, Sports, Culture and Technology, Japan; and by the Smoking Research Foundation.

References

1. Macgregor PF, Squire JA. Application of microarrays to the analysis of gene expression in cancer. Clin Chem 2002;48:1170–7.
2. Santacroce R, Ratti A, Caroli F, Foglieni B, Ferraris A, Cremonesi L, et al. Analysis of clinically relevant single-nucleotide polymorphisms by use of microelectronic array technology. Clin Chem 2002;48:2124–30.
3. Gentalen E, Chee M. A novel method for determining linkage between DNA sequences: hybridization to paired probe arrays. Nucleic Acids Res 1999;27:1485–91.
4. Huang JX, Mehrens D, Wiese R, Lee S, Tam SW, Daniel S, et al. High-throughput genomic and proteomic analysis using microarray technology. Clin Chem 2001;47:1912–6.

5. Frayling IM. Methods of molecular analysis: mutation detection in solid tumours. Mol Pathol 2002;55:73–9.
6. Hoque MO, Lee CC, Cairns P, Schoenberg M, Sidransky D. Genome-wide genetic characterization of bladder cancer: a comparison of high-density single-nucleotide polymorphism arrays and PCR-based microsatellite analysis. Cancer Res 2003;63:2216–22.
7. Wikman FP, Lu ML, Thykjaer T, Olesen SH, Andersen LD, Cordon-Cardo C, et al. Evaluation of the performance of a p53 sequencing microarray chip using 140 previously sequenced bladder tumor samples. Clin Chem 2000;46:1555–61.
8. Chizhikov V, Rasooly A, Chumakov K, Levy DD. Microarray analysis of microbial virulence factors. Appl Environ Microbiol 2001;67:3258–63.
9. Lucito R, Healy J, Alexander J, Reiner A, Esposito D, Chi M, et al. Representational oligonucleotide microarray analysis: a high-resolution method to detect genome copy number variation. Genome Res 2003;13:2291–305.
10. Foglieni B, Cremonesi L, Travi M, Ravani A, Giambona A, Rosatelli MC, et al. β-Thalassemia microelectronic chip: a fast and accurate method for mutation detection. Clin Chem 2004;50:73–9.
11. Cooper M, Li S-Q, Bhardwaj T, Rohan T, Kandel RA. Evaluation of oligonucleotide arrays for sequencing of the *p53* gene in DNA from formalin-fixed, paraffin-embedded breast cancer specimens. Clin Chem 2004;50:500–8.
12. Sassi AP, Paulus A, Cruzado ID, Bjornson T, Hooper HH. Rapid, parallel separations of d1S80 alleles in a plastic microchannel chip. J Chromatogr A 2000;894:203–17.
13. Sosnowski RG, Tu E, Butler WF, O'Connell JP, Heller MJ. Rapid determination of single base mismatch mutations in DNA hybrids by direct electric field control. Proc Natl Acad Sci U S A 1997;94:1119–23.
14. van Beumingen R, van Damme H, Boender P, Bastiaensen N, Chan A, Kievits T. Fast and specific hybridization using flow-through microarrays on porous metal oxide. Clin Chem 2001;47:1931–3.
15. Hokaiwado N, Asamoto M, Tsujimura K, Hirota T, Ichihara T, Satoh T, et al. Rapid analysis of gene expression changes caused by liver carcinogens and chemopreventive agents using a newly developed three-dimensional microarray system. Cancer Sci 2004;95:123–30.
16. Yanez L, Groffen J, Valenzuela DM. c-K-ras mutations in human carcinomas occur preferentially in codon 12. Oncogene 1987;1:315–8.
17. Maekawa M, Sugano K, Ushiama M, Fukayama N, Nomoto K, Kashiwabara H, et al. Heterogeneity of DNA methylation status analyzed by bisulfite-PCR-SSCP and correlation with clinico-pathological characteristics in colorectal cancer. Clin Chem Lab Med 2001;39:121–8.
18. Maekawa M, Taniguchi T, Tatebayashi C, Horii T, Takeshita A, Sugimura H, et al. Basic studies on mutation analysis of K-ras codon 12 by use of three-dimensional microarray system. Rinsho Byori 2003;51:306–12.
19. Verlaan-de Vries M, Bogaard ME, van den Elst H, van Boom JH, van der Eb AJ, Bos JL. A dot-blot screening procedure for mutated ras oncogenes using synthetic oligodeoxynucleotides. Gene 1986;50:313–20.
20. Sugano K, Kyogoku A, Fukayama N, Ohkura H, Shimosato Y, Sekiya T, et al. Methods in laboratory investigation. Rapid and simple detection of c-Ki-ras2 gene codon 12 mutations by nonradioisotopic single-strand conformation polymorphism analysis. Lab Invest 1993;68:361–6.
21. Wallace DC. Mitochondrial genetics: a paradigm for aging and degenerative diseases? Science 1992;256:628–32.
22. Finkelstein SD, Sayegh R, Christensen S, Swalsky PA. Genotypic classification of colorectal adenocarcinoma. Cancer 1993;71:3827–38.
23. Cerottini J-P, Caplin S, Saraga E, Givel J-C, Benhattar J. The type of K-ras mutation determines prognosis in colorectal cancer. Am J Surg 1998;175:198–202.
24. Al-Mulla F, Going JJ, Sowden ET, Winter A, Pickford IR, Birnie GD. Heterogeneity of mutant versus wild-type Ki-ras in primary and metastatic colorectal carcinomas, and association of codon-12 valine with early mortality. J Pathol 1998;185:130–8.
25. Andreyev HJ, Norman AR, Cunningham D, Oates J, Dix BR, Iacopetta BJ, et al. Kirsten ras mutations in patients with colorectal cancer: the 'RASCAL II' study. Br J Cancer 2001;85:692–6.

Glycobiology vol. 15 no. 9 pp. 887–894, 2005
doi:10.1093/glycob/cwi071
Advance Access publication on May 4, 2005

Polysialic acid facilitates tumor invasion by glioma cells

Masami Suzuki[1,3,4], Misa Suzuki[1,4], Jun Nakayama[1,5], Atsushi Suzuki[3,4], Kiyohiko Angata[4], Shihao Chen[4], Keiichi Sakai[6], Kazuki Hagihara[7], Yu Yamaguchi[7], and Minoru Fukuda[2,4]

[4]Glycobiology, Cancer Research Center, The Burnham Institute, La Jolla, CA 92037; [5]Department of Pathology, Shinshu University School of Medicine, Matsumoto 390-8621, Japan; [6]Department of Neurosurgery, Shinshu University School of Medicine, Matsumoto 390-8621, Japan; [7]Developmental Neurobiology Programs, Cancer Research Center, The Burnham Institute, La Jolla, CA 92037

Received on March 15, 2005; revised on April 26, 2005; accepted on April 27, 2005

Polysialic acid (PSA) is thought to attenuate neural cell adhesion molecule (NCAM) adhesion, thereby facilitating neural cell migration and regeneration. Although the expression of PSA has been shown to correlate with the progression of certain tumors such as small cell lung carcinoma, there have been no studies to determine the roles of PSA in gliomas, the most common type of primary brain tumor in humans. In this study, we first revealed that among patients with glioma, PSA was detected more frequently in diffuse astrocytoma cells, which spread extensively. To determine directly the role of PSA in glioma cell invasion, we transfected C6 glioma cells with polysialyltransferases to express PSA. In those transfected cells, PSA is attached mainly to NCAM-140, whereas the mock-transfected C6 cells express equivalent amounts of PSA-free NCAM-140. Both PSA negative and positive C6 cell lines exhibited almost identical growth rates measured in vitro. However, PSA positive C6 cells exhibited increased invasion to the corpus callosum, where the mock-transfected C6 glioma cells rarely invaded when inoculated into the brain. By contrast, the invasion to the corpus callosum by both the mock-transfected and PSA positive C6 cells was observed in NCAM-deficient mice. These results combined indicate that PSA facilitates tumor invasion of glioma in the brain, and that NCAM–NCAM interaction is likely attenuated in the PSA-mediated tumor invasion.

Key words: polysialic acid/glioma/tumor invasion/NCAM/polysialyltransferases

Introduction

Polysialic acid (PSA) is a unique carbohydrate of a linear homopolymer of α2,8-linked sialic acid (Finne, 1982). PSA is primarily attached to *N*-glycans of the neural cell adhesion molecule (NCAM) in neural cells (Finne, 1982; Edelman, 1984; Rutishauser and Landmesser, 1996; Kiss and Rougon, 1997; Kleene and Schachner, 2004), whereas it is attached to mucin-type glycoproteins in human breast carcinoma and leukemic cells (Martersteck *et al.*, 1996). Polysialylated NCAM is abundant in the embryonic brain. Most NCAM in the adult brain does not contain PSA, but polysialylated NCAM is continuously present in the hippocampus and olfactory bulbs, where neuronal generation persists in the adult (Edelman, 1984; Rutishauser and Landmesser, 1996; Kiss and Rougon, 1997; Kleene and Schachner, 2004).

The cDNAs-encoding polysialyltransferases have been cloned, and these enzymes are called ST8Sia IV (also called PST) and ST8Sia II (also called STX) (Livingston and Paulson, 1993; Eckhardt *et al.*, 1995; Nakayama *et al.*, 1995; Scheidegger *et al.*, 1995; Yoshida *et al.*, 1995). Both ST8Sia II and ST8Sia IV catalyze the transfer of multiple α2,8-linked sialic acid residues to a glycan containing NeuNAcα2→3/6Galβ1→4GlcNAc→R (Angata *et al.*, 2000). During development, the expression of *ST8Sia II* and *ST8Sia IV* genes is specifically regulated (Hildebrandt *et al.*, 1998a; Ong *et al.*, 1998). The amount of ST8Sia II is more significantly reduced postnatally compared with ST8Sia IV (Hildebrandt *et al.*, 1998a; Ong *et al.*, 1998). Mutant mice with ST8Sia II deficiency exhibited misguidance of infrapyramidal mossy fibers and the formation of ectopic synapses in the hippocampus. This altered hippocampus development was associated with higher exploratory drive (Angata *et al.*, 2004). Mutant mice with ST8Sia IV deficiency, on the other hand, bore a restricted phenotype involving an impairment of long-term potentiation in the hippocampal CA1 region (Eckhardt *et al.*, 2000). These results suggest that ST8Sia II and ST8Sia IV may differentially direct the synthesis of PSA in temporal and spatial-specific manners.

PSA has been found in various tumors including small cell and nonsmall cell lung carcinomas, multiple myeloma, neuroblastoma, and Wilms' tumor (Roth *et al.*, 1988; Van Camp *et al.*, 1990; Fukuda, 1996; Smith *et al.*, 1996; Hildebrandt *et al.*, 1998b; Seidenfaden *et al.*, 2000; Tanaka *et al.*, 2000). In both small cell and nonsmall cell lung carcinomas and multiple myeloma, the expression of PSA is correlated with tumor progression (Scheidegger *et al.*, 1994; Smith *et al.*, 1996; Hildebrandt *et al.*, 1998b; Tanaka *et al.*, 2000). In one particular study, small cell lung carcinoma cells expressing different amounts of PSA were isolated from H69 cell line by clonal dilution of cells. After subcutaneous inoculation of these tumor cells, tumor cells expressing PSA produced

[1]These authors contributed equally to this work.
[2]To whom correspondence should be addressed; e-mail: minoru@burnham.org
[3]Present address: Department of Obstetrics and Gynecology, Keio University School of Medicine, Tokyo 160-8582, Japan

more intracutaneous metastasis than tumor cells poorly expressing PSA, although a comparable amount of NCAM was expressed in these variants (Scheidegger *et al.*, 1994).

Gliomas are the most common type of primary brain tumors in humans. It is highly invasive in nature, but tumor metastasis to other organs is rare (Thorsen and Tysnes, 1997). To elucidate the mechanisms of glioma invasion and migration, transfections of various genes to glioma cell lines have been tested for tumor invasion and migration (Kaye *et al.*, 1986; Edvardsen *et al.*, 1994; Chicoine and Silbergeld, 1995; Thorsen and Tysnes, 1997; Owens *et al.*, 1998). In particular, the forced expression of NCAM-140 in glioma cell lines resulted in reduced migration when the glioma cells were inoculated into the brain (Edvardsen *et al.*, 1994) or assayed for migration through a reconstituted basal lamina, Matrigel (Chicoine and Silbergeld, 1995). However, no studies have addressed the direct roles of PSA in glioma invasion in the brain.

In this study, we first found that among the 44 patients with astrocytoma examined, PSA was detected in nine cases of the 30 NCAM-positive astrocytoma, in particular, a diffuse astrocytoma subtype which spreads extensively. ST8Sia IV and ST8Sia II transcripts were also detected in a recurred case of diffuse astrocytoma, which expressed PSA. We then assayed experimental tumor formation of C6 rat glioma cell line in the brain after transfection with ST8Sia II or ST8Sia IV cDNA to express PSA. Mock-transfected and PSA-positive C6 cell lines were inoculated into the brain of wild type and NCAM-deficient mice. The results obtained indicate that PSA expressed on glioma cells facilitates tumor invasion, most likely due to the attenuation of NCAM–NCAM interaction.

Results

Expression of PSA, ST8Sia II mRNA, and ST8Sia IV mRNA in human astrocytoma

Immunohistochemistry by using anti-NCAM monoclonal antibody demonstrated that NCAM was expressed along cytoplasmic processes of the tumor cells in 30 (68.2%) of 44 patients examined, irrespective of the histological grade of the tumor, that is, five cases (83.3%) of six pilocytic astrocytoma, 10 (66.7%) of 15 diffuse astrocytoma, 11 (68.8%) of 16 anaplastic astrocytoma, and four (57.1%) of seven glioblastoma multiforme. On the other hand, PSA was immunohistochemically detected in nine (30%) of 30 patients, which also expressed NCAM in the tumor cells; one case (20%) of pilocytic astrocytoma, four cases (40%) of diffuse astrocytoma, three cases (27.3%) of anaplastic astrocytoma, and one case (25%) of glioblastoma multiforme (Figure 1). Clinical records of the patients at the surgical operation revealed that four (44.4%) of nine PSA-positive patients were recurred cases, whereas five (23.8%) of 21 patients expressing NCAM alone were recurred cases. This result suggests that PSA expressed on the tumor cells was associated with recurrence of the disease. These results combined with the morphological examination of tumor cells suggest that PSA is expressed more frequently in those gliomas that spread extensively, which makes it difficult to remove all of the glioma cells in the first operation.

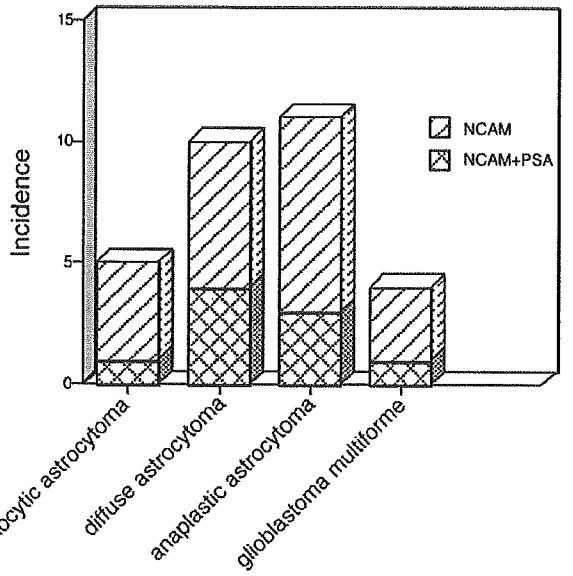

Fig. 1. Expression of polysialic acid (PSA) and neural cell adhesion molecule (NCAM) in human astrocytomas. Expression of NCAM and PSA was examined by using 123C3 anti-NCAM antibody and 5A5 anti-PSA antibody. Among NCAM-positive tumor cells, the numbers of PSA-positive tumor cells are also shown.

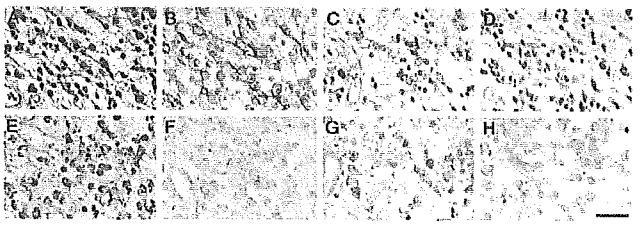

Fig. 2. Expression of polysialic acid (PSA) and ST8Sia II and ST8Sia IV transcripts in a recurred case of diffuse astrocytoma invading contralateral cerebral hemisphere through corpus callosum. The tumor stained with hematoxylin and eosin shows a protoplasmic astrocytoma proliferating in a loose microcystic matrix (**A**). In parallel sections, neural cell adhesion molecule (NCAM) was detected by 123C3 antibody (**B**), and PSA was stained by 5A5 antibody before (**C**) and after (**D**) endo-neuraminidase-*N* (endo-*N*) treatment. Parallel sections were also subjected to in situ hybridization by using antisense probes for ST8Sia IV (**E**) and ST8Sia II (**G**) and sense probes for ST8Sia IV (**F**) and ST8Sia II (**H**). All the photographs are shown in the same magnification (bar = 50 μm).

Indeed in one recurred case of diffuse astrocytoma, significant amounts of PSA (Figure 2C) as well as NCAM (Figure 2B) were detected in the cell surface and cytoplasmic processes of tumor cells, and the magnetic resonance imaging of this patient revealed that the recurred tumor mainly occupied the right frontal lobe of cerebrum and invaded the left frontal lobe through the corpus callosum. To determine whether two polysialyltransferases, ST8Sia II and ST8Sia IV, play a major role in the biosynthesis of PSA in the glioma cells, we analyzed serial tissue sections of the above case by in situ hybridization using specific RNA probes for ST8Sia II and ST8Sia IV. The results show that both ST8Sia II (Figure 2G) and ST8Sia IV (Figure 2E)

transcripts were detectable in the tumor cells, and ST8SiaIV apparently plays a major role in the polysialylation of this tumor.

Isolation of C6 glioma cells expressing PSA

To directly demonstrate the roles of PSA in glioma invasion, we measured tumor formation of C6 glioma cells after the cells were transfected with ST8Sia II or ST8Sia IV cDNA. After transfecting with pcDNA3-ST8Sia II or pcDNA3-ST8Sia IV, clonal cell lines expressing PSA were isolated, resulting in C6-ST8Sia II and C6-ST8Sia IV. As shown in Figure 3A, C6-ST8Sia II and C6-ST8Sia IV were positive for both PSA and NCAM, whereas the mock-transfected C6 cell line was positive only for NCAM. The results also demonstrated that all three cell lines express almost identical amounts of NCAM as assessed by fluorescence activated cell sorter (FACS) analysis.

Western blot analysis of C6, C6-ST8Sia II, and C6-ST8Sia IV illustrates that PSA-containing proteins migrated as a large heterogeneous molecular mass of 170–240 kDa (Figure 3B). After removing PSA by endoneuraminidase-*N* (endo-*N*) digestion, NCAM molecules migrated at almost the same position as the NCAM of C6 cells and NCAM-140 expressed on HeLa cells. The results also show that a small amount of NCAM-180 is expressed although this band might also represent a dimer of NCAM-140 (Angata *et al.*, 1997). These results indicate that most PSA is attached to NCAM-140 in C6-ST8Sia II and C6-ST8Sia IV. NCAM was estimated to contain 20–40 sialic acids and 10–35 sialic acids for C6-ST8Sia II and C6-ST8Sia IV cells, respectively, using the procedure described previously (Angata *et al.*, 1998). Polysialylation by ST8Sia IV was less efficient than that by ST8Sia II, probably because C6 cells that express a large amount of PSA after transfection by ST8Sia IV tend to detach from the substratum.

Expression of PSA does not increase cell growth

To determine whether the expression of PSA facilitates tumor cell growth in vitro, the cells were plated at low density and the growth rate was determined. The results demonstrated that the expression of PSA did not alter the rate of tumor cell growth when assessed by a cell proliferation assay in vitro (Figure 4).

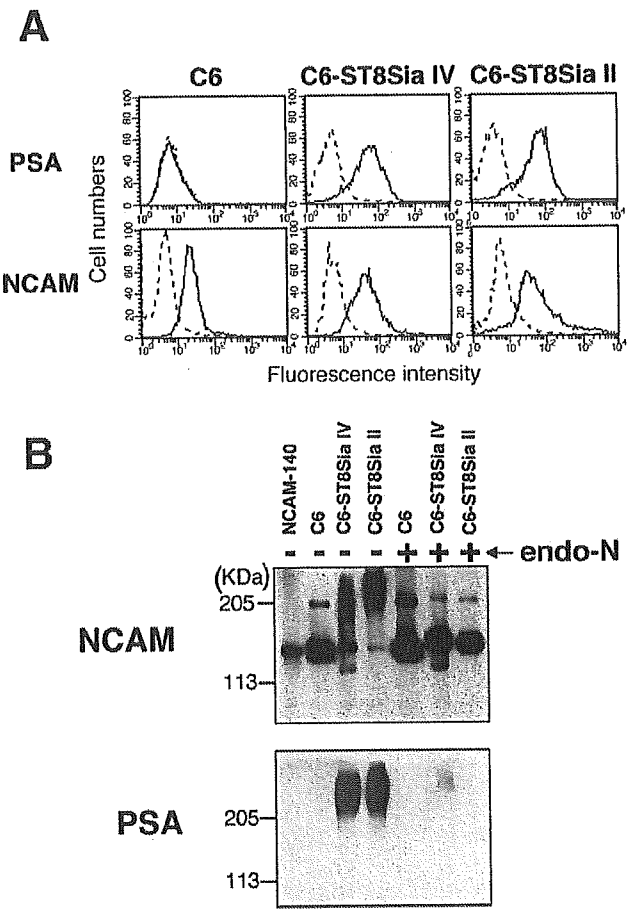

Fig. 3. Expression of neural cell adhesion molecule (NCAM) and polysialic acid (PSA) in C6 cells and C6 cells transfected with ST8Sia IV or ST8Sia II cDNA. **(A)** The cells were stained with 12F8 anti-PSA antibody or 5B8 anti-NCAM antibody followed by fluoroscein isothiocyanate-conjugated secondary antibody (anti-rat IgM for PSA and anti-mouse IgG for NCAM) and subjected to flow cytometric analysis. Dotted lines indicate a control omitting the primary antibodies. **(B)** The cells shown in panel A were subjected to western blot analysis before (–) and after (+) endoneuraminidase-*N* (endo-*N*) treatment. NCAM and PSA were detected with the same antibodies used in panel A. HeLa cells expressing NCAM-140 (NCAM-140) were treated in the same manner.

Tumor invasion of C6 glioma cells expressing PSA

Although many of invasion studies were carried out in vitro using for example, Matrigel, this assay is not suited for studying invasion in the brain because substantial differences exists in the extracellular components between Matrigel and the brain (Yamaguchi, 2000). We thus opted to utilize in vivo invasion assay.

When the mock-transfected C6 glioma cells were inoculated into the caudate putamen, tumor cells gradually spread to surrounding tissue and then mostly to the cerebral cortex (Figure 5A and B), consistent with C6 glioma derived from diffuse fibrillary astrocytoma (Thorsen and Tysnes, 1997). When PSA-expressing C6-ST8Sia II cells were inoculated in the same manner, more tumor invasion was observed, in particular, to the corpus callosum (Figure 5D–F). These tumor cells were positive for PSA, and the positive staining was abolished by pretreatment with endo-*N* (Figure 5G and H). It is noteworthy that each glioma cell highly extended along myelinated fibers in the corpus callosum (Figure 5E insert), in contrast to spindle shape of the mock-transfected C6 cells (Figure 5B insert). Similar results were obtained for PSA-expressing C6-ST8Sia IV cells (Figure 6). By contrast, C6 cells negative for PSA scarcely exhibited invasion to the corpus callosum under the same conditions (Figures 5B and C and 7). Almost identical results were obtained on more than two independently cloned cells.

Invasion to corpus callosum in the absence of NCAM

The above results showed that the invasion of PSA-expressing C6 cells to the corpus callosum may be one of the important